C.P. No. 1264

C.P. No. 1264

MINISTRY OF DEFENCE (PROCUREMENT EXECUTIVE)

AERONAUTICAL RESEARCH COUNCIL

CURRENT PAPERS

On the Influence of Camber and Non-Planar Vortex Wake on Wing Characteristics in Ground Effect

By

B. Maskew, Ph.D., D.C.Ae., C.Eng., A.F.R.Ae.S.,

Department of Transport Technology,

Loughborough University of Technology

LONDON· HER MAJESTY'S STATIONERY OFFICE

1973

PRICE 95p NET

C.P. No. 1264*
October, 1971

ON THE INFLUENCE OF CAMBER AND NON-PLANAR VORTEX WAKE ON WING CHARACTERISTICS IN GROUND EFFECT≠

by

B. Maskew, Ph.D., D.C.Ae., C.Eng., A.F.R.Ae.S.,

Department of Transport Technology,

Loughborough University of Technology

SUMMARY

This note examines the theoretical influence of camber and non-planar wake on the chance of lift, vortex drag and centre of pressure of a wing with ground effect.

Calculations are performed for both two and three-dimensional potential flows for ground effect conditions which are fairly representative of a conventional aircraft in a high-lift configuration. The two-dimensional problem is evaluated using a multivortex method on two aerofoil sections at ground heights $h/c = 1.0$ and 0.5; a flat plate section is considered over a range of incidence ($C_{\ell_\infty} = 0$-3.0) and a bent plate section at zero incidence for a range of plain flap deflections ($\delta_f = 0°$ to $60°$). The three-dimensional results are obtained using an arbitrary geometry quadrilateral vortex-ring method with a vortex wake relaxation iterative scheme and a ground image vortex system. The wing is untapered with an aspect ratio of 4 and a full span plain flap of $0.25c$. It is set at an incidence of 10° with a height above ground (quarter standard mean chord) h/b value of 0.15. Two angles of sweepback are considered (0° and 45°) and the results are presented for a range of flap deflections (0° to 30°). Only a small number of vortex-ring elements (i.e., 3×8) is used in the calculations in order to keep computer time down (the aim is to demonstrate the effects rather than give accurate results). Even so the results are expected to be reasonably accurate.

The/

---

* Replaces A.R.C.33 950

≠ This is the third report on a programme of research into lifting surface methods and demonstrates the application of numerical potential flow methods to the calculation of highly cambered wing characteristics in ground effect.

The calculated results demonstrate the importance of including the influence of camber, incidence and non-planar wake in practical ground effect calculations; whereas existing three-dimensional methods generally give favourable ground effect (viz., increase in lift and decrease in vortex drag), these results show that the effect can be unfavourable in terms of lift and less favourable in terms of vortex drag.

The Quadvort method with the wake relaxation iterative scheme is seen to be a potentially powerful tool for handling complicated flow interference problems of this type.

LIST OF CONTENTS

1.0 INTRODUCTION

When an aircraft is moving close to the ground its aerodynamic characteristics - lift, drag and centre of pressure - can be appreciably modified from their free air values. These modifications must be taken into account when calculating the aircraft's performance and stability and control characteristics for take-off and landing and particularly for S.T.O.L.

Consideration of the wing lifting system image in the ground plane (e.g. 2.2.1) leads readily to the generally accepted qualitative nature of ground effect; namely, that the lift increases and the vortex drag decreases. Provided the incidence and camber are small and the wing is not too close to the ground these effects can be fairly reliably calculated using data sheets[1,2]. In fact, existing theoretical work[3,4,5,6,7,21] on ground effect in three-dimensional flow is based on the assumption that the wing and vortex wake lie essentially parallel to the free stream direction. Normally, however, when an aircraft is close to the ground it is in a high lift configuration with large camber and large incidence and the vortex wake can be considerably displaced from the wing plane. Also, during the take-off and landing ground roll, many aircraft have quite small ground heights (e.g. Table 1). For such practical problems the application of existing methods is not reliable, in fact Reference 1 quotes a $\pm$ 30% tolerance to cover such cases. Qualitatively it is known that ground proximity can reduce flap lifting effectiveness. Indeed, Tomotika[8] has shown that in two-dimensional flow ground effect can actually reduce lift for large cambers (circular arc). Similar results were obtained by Rubbert[9] using a two-dimensional multi-vortex method on a bent plate aerofoil.

The purpose of the present note is to demonstrate the theoretical influence of camber and non-planar vortex wake on the effect of ground proximity on lift, vortex drag and centre of pressure of a wing. This work forms part of an investigation into arbitrary lifting surface methods and is published separately here in view of the general lack of information on the subject and also in view of current interest[10,11,12] in non-planar wakes and the wake roll-up problem.

In this note a discussion of the general qualitative nature of ground effect (Section 2.0) is followed by an evaluation of the problem in two-dimensional flow (Section 3.0). These provide a background to the main three-dimensional calculations

(4.0) involving a wing with full span plain flap. Two angles of sweepback (0^{o} and 45^{o}) are considered and the calculated results are presented for a range of flap deflections.

Potential flow conditions are assumed, so the effect of flow separation over the flap is excluded. However, for real flow results it is conceivable that a potential flow flap deflection can be empirically derived, which is equivalent to an actual flap deflection (say on the basis of lift generated). The calculations should be directly applicable to wings having boundary layer control but not to the extent of supercirculation at this stage. The influence of part span flaps, taper ratio and dihedral on ground effect are not included in the present note (though the computer program can handle these). Also excluded is the effect of wing thickness - but this effect should be small at the ground heights considered here.

The method used here for the three-dimensional calculations is an extended version of the quadrilateral vortex-ring method (Quadvort) outlined in Reference 13. Quadvort is itself an extension of the vortex lattice method[14, 15, 16], the validity of which for evaluating ground effect for planar wing and vortex-wake has already been demonstrated[7] in a comparison with Saunders[6] kernel function method and also experiment. For the present work the Quadvort computer program has been extended to include a vortex wake relaxation iterative procedure which is briefly outlined in 4.1.2 and which is basically similar to wake relaxation methods described by Butter & Hancock[10], Hackett & Evans[12] and Belotserkovskii[11], except it is now attached to an arbitrary cambered lifting surface method (with the facility for considering a discontinuous trailing edge or starting line). Also the program now includes the facility for scanning the image wing (or wings) in the ground plane. This program can thus be applied to the non-planar wake problem of multi-cambered plates (e.g. wing-flaps-tailplane) in and out of ground effect and also in the presence of tunnel walls.

The computer program (which is not up to production standard) currently requires 29K words of core. A case involving two wake iterations, 24 surface elements, 11 trailing vortices (each with 10 straight line segments) and one plane of symmetry, takes 9 minutes for a free air calculation and 17 minutes for ground effect (mill times) on the ICL 1904A computer. The program can currently handle up to 50 surface elements (on half a symmetrical problem) on three components (e.g. wing plus tailpane plus simple fuselage or simple wing and tailplane in a wind tunnel). An extension for handling more elements and components would be straight forward.

2.0 QUALITATIVE NATURE OF GROUND EFFECT

2.1 General

Before discussing the calculation of ground effect in the general case, it is instructive - in the sense of gaining physical insight - to reassess its qualitative nature at small incidence, using a simple model, and then to extend this assessment to the case of large incidence (or large surface slope).

Consider a flat plate wing represented by a vortex lattice. The sketches below (1, 2) show a section of the model using just one vortex but the same principle applies as in the case of more vortices. The evaluation of the forces on the plate can be regarded in two stages.

i) the vortex strengths are solved after applying the boundary condition that the normal component of free stream velocity at certain surface control points is cancelled by the normal component of total induced velocity (i.e. from surface and trailing vortices) see Sketch 1.

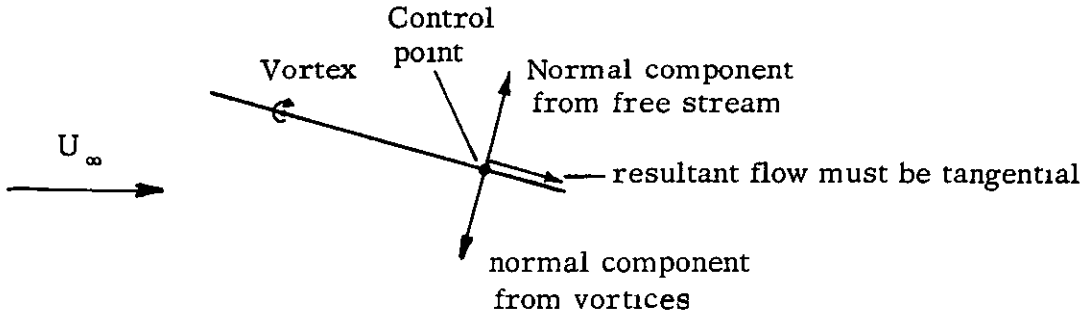

SKETCH 1 SOLUTION OF VORTEX STRENGTH IN FREE AIR

ii) the force on each bound vortex is proportional to the vector product of the local velocity and the vorticity vector. (For a flat plate at small incidence in free air the local velocity is essentially that of the free stream plus a downwash from the trailing vortices).

When the wing approaches the ground it effectively comes under the influence of its own reflection in the ground plane. The image (i.e. of the vortex lattice system) has three effects:

a) it contributes a normal velocity component to the boundary condition equations (i) and hence modifies the vortex strength solution (and forces). (Sketch 2).

b) it contributes to the local velocity at each vortex (ii) and this further modifies the forces. (Sketch 2).

c) it modifies the shape of the vortex wake.

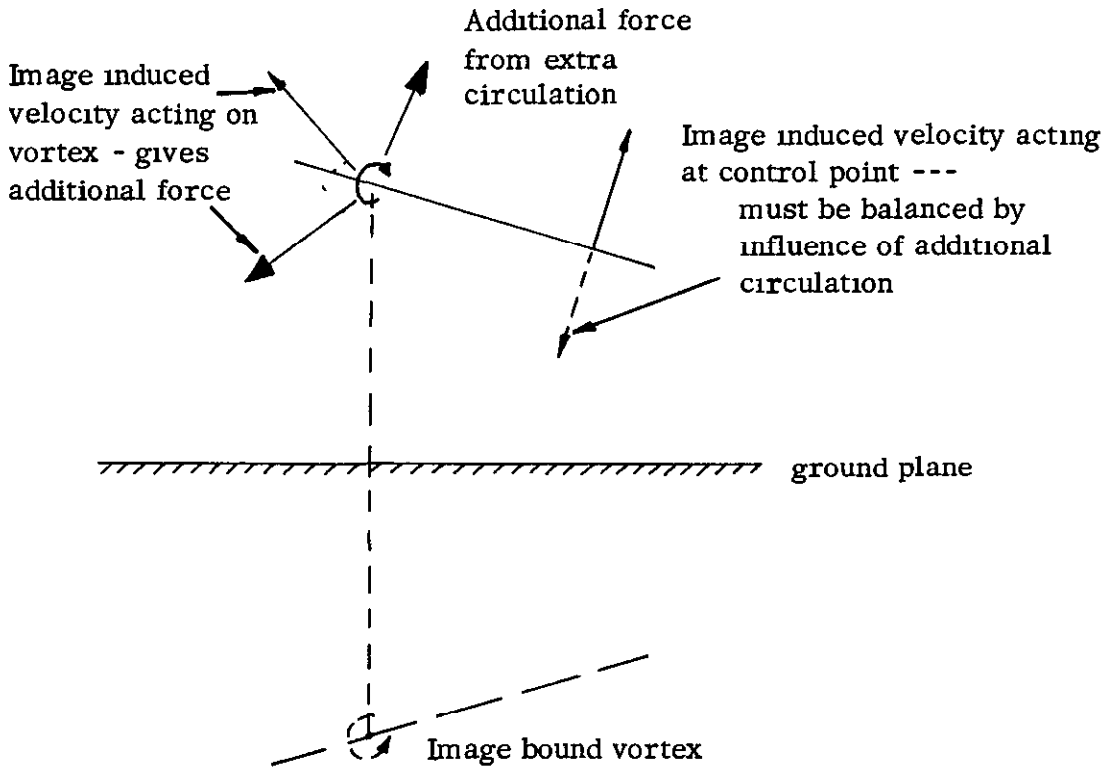

SKETCH 2 ADDITIONAL VELOCITIES FROM GROUND IMAGE AND THEIR GENERAL EFFECT

2.2 Small Incidence and Camber

Consider the separate contributions to these effects from the bound and trailing vortex images for a wing with small incidence and camber.

2.2.1 Influence of trailing vortex images

The image trailing vortices induce over the whole wing an upwash and a sidewash (Sketch 3) ; these increase as ground height decreases and vary across the span giving an induced twist effect.

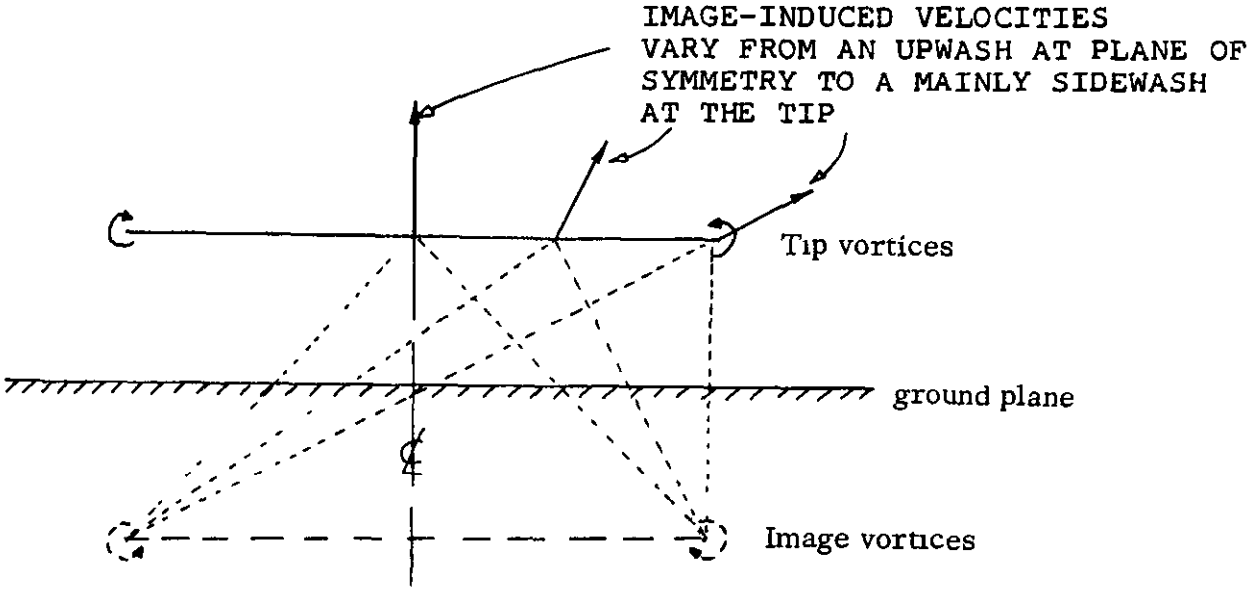

SKETCH 3 SECTION THROUGH WING WAKE SHOWING MAIN EFFECT OF IMAGE TRAILING VORTICES

The main effect comes from the upwash which:

i) tends to increase all vortex strengths (2.1.a))

ii) gives a negative increment in vortex drag (vector product of upwash velocity and local vortex vector (2.1.b))

The sidewash tends to reduce lift on swept wings (vector product of local sidewash velocity and vorticity vector (2.1.b)). Thus the increment in lift should decrease with sweepback.

The image trailing vortex system displaces the vortex wake vertically away from the ground and horizontally away from the plane of symmetry - see the velocity vector at the tip vortex in Sketch 3. This modification should only have a small effect on the wing itself but could considerably affect the downwash at, say, the tailplane. (Indeed, in wind-tunnel tests of ground effect, erroneous longitudinal trim characteristics can be obtained since the presence of the tunnel walls - and hence further image vortices - tends to suppress this sideways movement of trailing vortices and also changes their vertical position.)

2.2.2 Influence of bound vortex images

The image bound vortices have two main effects which vary across the chord of the wing - giving an induced camber effect - and which vary with height above ground:

a) the boundary condition equations (2.1.a) are modified by components of the normal induced velocity which are mainly upwards at the rear and downwards at the front of the wing - thus the vortex strengths tend to increase at the rear and decrease at the front, giving a rearward shift in centre of pressure.

b) They contribute to the induced velocities at the bound vortex locations (2.1.b);

   i) components parallel to the ground plane tend to reduce the lift force on a vortex

   ii) components normal to the ground plane can give rise to an induced drag.

In addition they have a local influence on the trailing vortex wake shape tending to increase the initial upward movement near the trailing edge and - on swept wings - increasing the initial outward movement.

2.3 Large Incidence and Camber

2.3.1 Influence of surface slope

The points discussed so far essentially still apply in the case of large incidence and camber but the inclination of the surface with respect to the ground plane modifies the effect.

a) For a given height of the wing quarter standard mean chord above the ground, the rear part of the vortex image system - including the trailing vortices (but not necessarily the tip vortex - see discussion in 4.2.4) - is closer to the actual wing and tends to reduce the effective h/b ratio (Sketch 4). This is particularly so at the tips of a swept wing.

b) The effect of induced upwash on the vortex strength solution (i.e., from the boundary condition equations (2.1.a) decreases as the surface slope to the ground increases - the effective part is the component normal to the surface (Sketch 4). Hence there is less increase in circulation from upwash.

c) The component of induced velocity parallel to the ground plane now contributes to the normal velocity at control points and thus affects the vortex strength solution, e.g., the forward induced velocity from image bound vortices gives a downward component relative to the surface and hence tends to reduce

circulation (sketch 4) (and on sweptback wings this downward component is increased by the sidewash velocity from image trailing vortices).

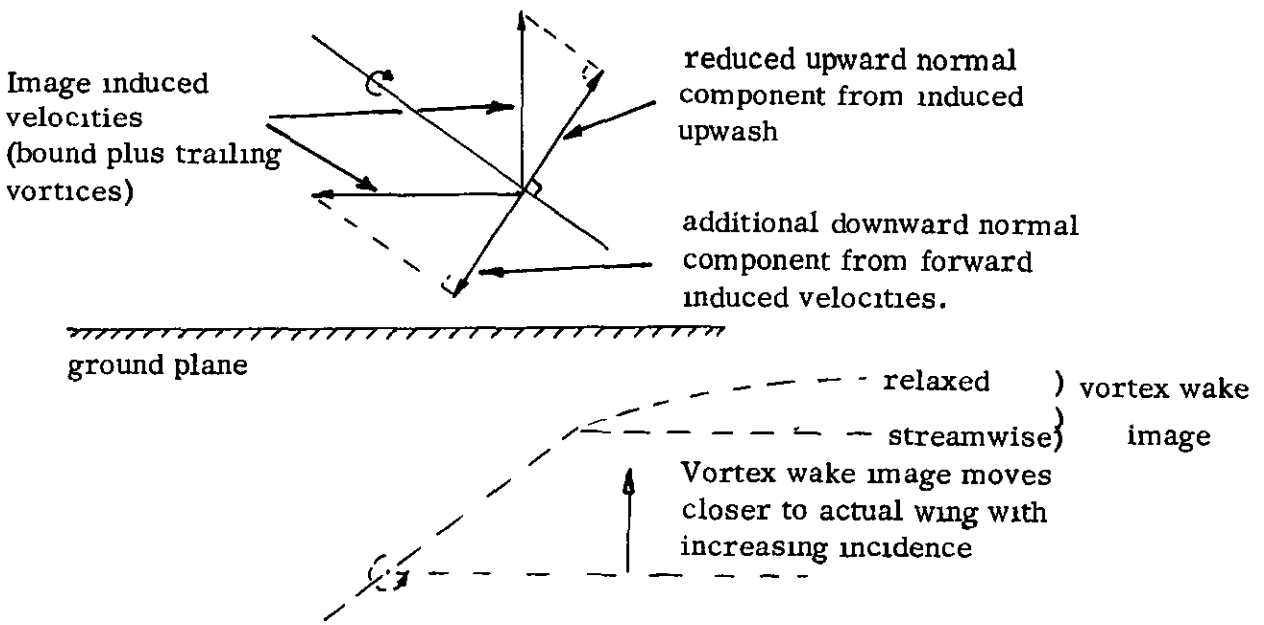

SKETCH 4 INFLUENCE OF SURFACE SLOPE IN GROUND EFFECT

2.3.2 Influence of Non-Planar Wake

Clearly in free air and at large incidence and camber, the true vortex wake lies below the streamwise plane from the trailing edge (- except for the powerful tip vortex (4.2.4)). This is still true in ground effect, though the wake is displaced upwards from its free air position. Thus the image of the true vortex wake is closer to the actual aerofoil than an assumed free streamwise wake (Sketch 4) and should therefore tend to give a smaller h/b effect.

2.3.3 Summary of Non-Planar Effects

The overall non-planar effect is complicated: on the one hand the image induced velocities tend to increase (2.3.1.a) and 2.3.2) and on the other their effectiveness - as far as lift is concerned - reduces (2.3.1.b and c)). However, it seems probable that the lift increment should be smaller than that calculated from linear ground effect theory. On a flapped wing the probable loss in lift with large surface slope would occur over the flap and would tend to move the centre of pressure forward (i.e. opposing the rearward shift with ground proximity which applies at small incidence and camber - 2.2.2a)).

In calculating the changes in the aerodynamic characteristics with ground effect for non-planar geometry, the non-planar effects in free air must also be accounted for, e.g., the trailing vortex induced downwash will also have reduced effectiveness owing to the increased surface slope.

3.0 EVALUATION OF GROUND EFFECT IN TWO-DIMENSIONAL FLOW

3.1. General

Two-dimensional theory can be usefully employed in order to gain further insight into the influence of camber and incidence on ground effect. In this section the effect of incidence is first considered and a simple theory derived. This is followed by an evaluation of the effect of camber which includes calculated results from a multi-vortex method. (These results provide a useful background to the three-dimensional calculations which follow in Section 4.0).

3.2 Effect of Incidence

3.2.1 Simple Theory

Consider again the single vortex model shown in Sketch 1 (Section 2.1). It will be recalled that the lifting effects of the flat plate in free air are correctly represented when the vortex is placed at the 0.25c point and the boundary condition of tangential flow specified at the 0.75c point.

This gives the free air circulation:

$$\Gamma_\infty = \pi c U_\infty \sin\alpha \qquad (1)$$

The local velocity at the vortex is of course the free stream value U_∞ :

$$\text{Hence} \quad C_{\ell_\infty} = \frac{2\Gamma_\infty}{U_\infty c}$$

$$\text{or} \quad C_{\ell_\infty} = 2\pi\sin\alpha \qquad (2)$$

In ground effect the two contributions from the image bound vortex noted in 2.2.2 can now be evaluated (at least for the simple model) - see Appendix.

a) The modification to the boundary condition gives a circulation in ground effect:

$$\Gamma_g = \pi c U_\infty \sin\alpha \left\{ 1 + \left\{ \tfrac{1}{4} \left(\frac{c}{h}\right)^2 - \frac{c}{h}\sin\alpha \right\} / \left\{ 4 - \frac{c}{h}\sin\alpha \right\} \right\}$$

or from equation (1):

$$\frac{\Gamma_g}{\Gamma_\infty} = 1 + \left\{ \frac{1}{4}\left(\frac{c}{h}\right)^2 - \frac{c}{h} \sin\alpha \right\} \Big/ \left\{ 4 - \frac{c}{h} \sin\alpha \right\} \qquad (3)$$

$$= F, \text{ say}$$

Thus at a fixed ground height h there is no ground effect on circulation when $\alpha = \sin^{-1}\left\{\frac{c}{4h}\right\}$ - say the neutral incidence (Sketch 5); at this incidence the image induced velocity is tangential to the ~~wing~~ surface at the 0.75c point (at least for this simple model; however, a similar neutral incidence could be defined for the general case). For smaller incidence than this the image induces an upwash at the control point and thus Γ must increase to maintain tangential flow and vice-versa for larger incidence. Alternatively, at a fixed incidence α there is zero ground effect on circulation for a height $h/c = 1/4 \sin\alpha$ - say the neutral height (see Fig. 1b); at a smaller height than this the image vortex induces an upwash at the control point and thus Γ must increase and vice-versa for a larger ground height.

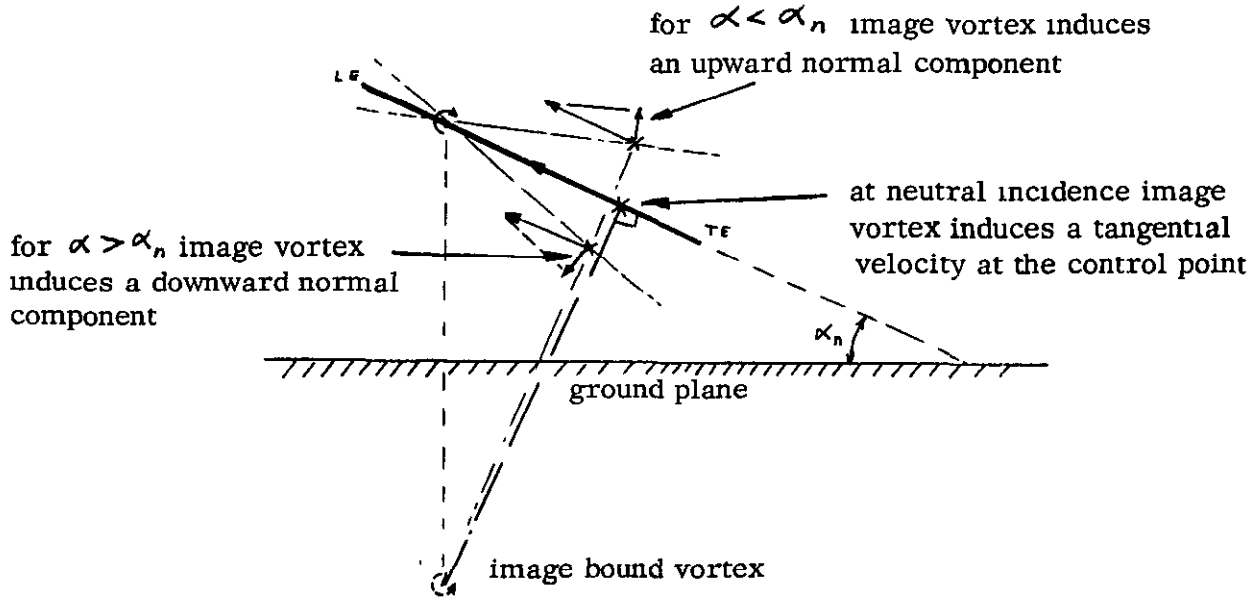

SKETCH 5 EFFECT OF INCIDENCE ON BOUNDARY CONDITION FOR CIRCULATION

b) The local velocity at the bound vortex becomes:

$$U_g = U_\infty - \frac{\Gamma}{4\pi h}$$

Thus the lift on the bound vortex is (Appendix) :

$$C_{\ell_g} = 2\pi \sin\alpha \, F \left\{ 1 - \frac{F}{4} \frac{c}{h} \sin\alpha \right\}$$

where F is defined in equation (3).

Or from equation (2) :

$$\frac{C_{\ell_g}}{C_{\ell_\infty}} = F \left\{ 1 - \frac{F}{8\pi} \frac{c}{h} C_{\ell_\infty} \right\} \qquad (4)$$

- - - - -

i.e. even when F = 1 (i.e no change in circulation) there is a reduction in C_ℓ in ground effect. Thus a neutral ground effect for C_ℓ still requires an increase in circulation (Figure 1.b).

In the limit at zero incidence equation (4) becomes:

$$\frac{C_{\ell_g}}{C_{\ell_\infty}} = 1 + \left(\frac{c}{4h}\right)^2 \qquad (5)$$

i.e. a favourable ground effect on lift.

Equation (4) is plotted in Figure 1a for two ground heights and shows clearly the importance of including the incidence effect (or - more generally - the effect of surface slope) at small ground heights; whereas a small incidence ground effect theory (e.g. equation 5) would give a large increase in C_ℓ near the ground (e.g. 25% at h/c = 0.5, which is fairly typical for aircraft static ground height (Table 1)), at large incidence (or large C_{ℓ_∞}) the lift can actually decrease. As incidence (or C_{ℓ_∞}) increases, the neutral point for $C_{\ell_g}/C_{\ell_\infty}$ occurs at a lower height above ground. This fact is made clearer in Figure 1.b where the boundary limits - according to equation (4) - are shown. For comparison, Figure 1.b also shows the neutral boundary for circulation (according to equation (3)) ; as expected from equation (4), the neutral boundary for circulation occurs at a higher C_{ℓ_∞} for a given h/c than the corresponding lift boundary.

3.2.2 Multi-vortex calculations

The multi-vortex method uses the two-dimensional basis for the vortex lattice method[14, 15, 16] and in effect applies the simple one-vortex principle (3.2.1) to a large

number of equal elements of chord. This method has been used by Rubbert[9] and Licher[21] to evaluate ground effect for flat plates at incidence and has shown excellent agreement with flat plate results from Tomotika's[17] transformation method over a wide range of incidence and ground height.

In the present work the multi-vortex method has been applied to the flat plate at incidence problem using 27 equispaced vortices, and the $C_{\ell_g}/C_{\ell_\infty}$ results are plotted in Figure 1a against C_{ℓ_∞} (i.e. incidence) in comparison with the simple theory (equation (4)). At a height above ground h/c = 1.0 the two lines are essentially the same; at the smaller height h/c = 0.5, the single vortex theory overestimates the effect by 2 to 4%. Results obtained using just three vortices gave no plottable difference from the 27-vortex results.

For ground heights down to at least the order of h/c = 0.5 it would appear from these calculations that the ground effect on a flat plate over a wide range of incidence can be adequately represented using a small number of vortices and that equation (4) represents a good estimate in this range.

3.3. Effect of Camber

3.3.1 Circular arc camber line

The multi-vortex method (using 50 equally spaced vortices on the camber line) has been applied to a circular arc aerofoil (camber = 0.053c) in ground effect and the results are given in Figure 2 in comparison with those from Tomotika's work[8]. The agreement is excellent for both lift and pitching moment.

Note that the ratio $C_{\ell_g}/C_{\ell_\infty}$ first decreases as the aerofoil approaches the ground then, when quite close to the ground, the lift starts to increase again. In Tomotika's[8] note a number of cambers are considered and the turn over point for $C_{\ell_g}/C_{\ell_\infty}$ occurs closer to the ground as camber increases. This is the same tendency as is seen in Figure 1b as incidence (C_{ℓ_∞}) increases and underlines the equivalent nature of surface slope and camber (for the lift effects at least).

3.3.2 Plain flap

The excellent agreement with the circular arc results from the transformation method gives confidence to the application of the multi-vortex method to more useful camber lines, e.g. a plain flapped aerofoil. Accordingly, calculations have been performed for a 0.25c flap over a range of deflections using 27 vortices evenly distributed

over the surface. Incidence is zero throughout.

The results are plotted in Figure 1a for two ground heights in comparison with the flat plate results (3.2.3). At the larger ground height (h/c = 1.0) the camber reduces the value of $C_{\ell_g}/C_{\ell_\infty}$ at a given C_{ℓ_∞} by the order of only 2%; closer to the ground (h/c = 0.5) the camber results are 5 to 6% below those from the flat plate. The camber results lie further away from the simple theory line (equation (4)) compared with the flat plate results.

In Figure 3 the lift is plotted against flap deflection for various ground heights; this figure shows the non-linear characteristics (arising from camber and ground effect) calculated by the multi-vortex method even for free air conditions (where the non-linearity arises entirely from the camber). The rate of increase in lift with flap deflection is seen to fall rapidly as the ground is approached.

Further flapped aerofoil calculations were performed using just three vortices at a ground height h/c = 0.6 and incidence 10^o (conditions corresponding to those for the three-dimensional calculations in Section 4.0). These results have been compared with 27 vortices results. The pressure distributions are shown in Figure 4. The agreement is remarkably good; the main deviation occurs at the peak suction at the flap hinge line. Table 2 gives the lift and centre of pressure values (note these are derived from circulations and not from the integrated pressure distribution). The agreement is seen to be excellent; the largest difference in C_ℓ is 1.08% for the 30^o flap in ground effect and the corresponding shift in centre of pressure is only 0.2% c. (At smaller ground heights the differences would be greater since the influence of the deflected flap bound vortices (both actual and image) is missing in the three vortex case - the last vortex falls on the hinge line and only the last control point dictates the tangential flow down the flap.) Note also in table 2 that the rearward shift in centre of pressure with ground effect for $\delta_f = 0^o$ is practically eliminated for $\delta_f = 30^o$ (see also 2.3.3).

From these results it is clear that three vortices are adequate in representing the influence of camber in ground effect at this ground height (h/c = 0.6) at least.

4.0 EVALUATION OF GROUND EFFECT IN THREE-DIMENSIONAL FLOW

4.1 General

The calculation method used here is briefly outlined in 4.2 which also includes

some observations from cases run so far (these cases are reported on more fully in reference 22). Although these observations are not directly concerned with ground effect, they do provide some useful background to the calculation of vortex wake roll-up which is used in the present calculations.

Details of the model used for the calculation are given in 4.3 and this is followed by a discussion of the calculated results in 4.4.

4.2 Calculation Method

4.2.1 Basis

The basic method used here is essentially an extension of the vortex lattice method [14,15,16] and is outlined in References 13 and 22. Briefly, the vortex sheet which replaces the lifting surface and wake in classical theory is here represented by a distribution of quadrilateral vortex rings (hence the method is referred to as Quadvort). A control point is selected in each vortex ring in turn and the boundary condition of tengential velocity (i.e. free stream plus vortex induced) is specified. Since at this stage the vortex strengths are unknown, a set of linear simultaneous equations is formed. The solution (i.e. the vortex-ring strength) of these equations is accomplished here by a successive orthogonalisation procedure [13,22]. Once the vortex-ring strengths are known, forces and moments and the velocity vector at any point in the field of flow can be calculated. When evaluating the force on a vortex the method of calculating the local velocity now differs from that given in Reference 13. Instead of interpolating between neighboring control point values each local velocity is now calculated directly by summing all the vortex induced velocities acting at the vortex mid-point and adding the free stream velocity. The resulting force and force distributions, obtained from summing the vector products of local velocities and vortex vectors (pp. 14 Reference 13) now include reasonably accurate values for vortex drag [22] as well as lift provided the vortex system is inset from the wing tip.

The Quadvort computer program has now been extended (from that outlined in Reference 13) to include a wake relaxation iterative scheme, which is outlined below, and also to include the influence of a ground image. Thus the method now takes into account all those influences discussed in 2.0 and 3.0.

4.2.2 Wake relaxation procedure

A basic solution for the vortex-ring strength is first calculated using the assumption of a streamwise wake from the actual trailing edge. Using this solution each trailing vortex is relaxed in turn, starting at the tip and working inboard.

In relaxing a vortex the calculation starts at the trailing edge and proceeds along the vortex in small straight line segments, the direction of each segment being determined by the local velocity vector. This vector is the sum of the free stream velocity and the total induced velocity from surface and wake vortices including their reflections in the plane of symmetry and ground - if present - but excluding the contribution from the (actual) trailing vortex being relaxed.

When all the vortices have been relaxed the matrix of influence coefficients (which is stored during the first solution) is modified for the change in vortex wake contribution and a second vortex solution obtained and so on.

4.2.3 *Convergence of the iteration*

In the results obtained so far there has been little change in vortex wake shape and force and moment characteristics after two iterations (even in the case of a wing with part span flap and tailplane [22]). However, the final shape of the vortex wake is affected by the segment length used (but mainly in the rolling up region); only with vanishingly small segment lengths will this be corrected, but at considerable expense in computer time. An extrapolation procedure is being considered to try to alleviate this problem [22]. In any case, although the vortex wake roll up is not completely represented (especially with large segments) the model is sufficiently close for the error in induced velocity at points removed from the roll-up region (e.g. at the tail plane) to be small.

However, if too large a segment length is used and a complicated wake is being calculated (e.g. that from a part span flap or a small aspect ratio wing tip (4.2.4)) then the wake can diverge after a few segment-lengths downstream from the trailing edge. A segment length/distance-between-vortices ratio of the order of unity has been found satisfactory so far.

4.2.4 Tip vortices

Early results obtained from the program showed that the tip of even large aspect ratio wings at large incidence and also the free edges of flaps at large deflections, inclined to behave like small aspect ratio wings, in that the edge trailing vortices were leaving the surface in more or less a free streamwise direction. Indeed it has long been known that at high incidence vortex sheets emanate from the side edges of wing. Accordingly a similar model to that used by Ermolenko [18] for small aspect ratio wings has been included in the program allowing vortices to spring freely from side edges. In Ermolenko's model the vortices proceed downstream to infinity in straight lines the direction of which are determined by the local flow angle at points above the trailing edge.

In the present model the complete velocity vector is calculated at points along each vortex and the vortices are allowed to roll round each other (Figure 5). It has since been found that Belotserkovskii [14] has extended his flat plate vortex lattice method in a similar manner [11] and has shown excellent agreement with experiment for the non-linear characteristics of small aspect ratio rectangular wings over a wide range of angle of attack.

The present method has also been applied to a very small aspect ratio (0.25) wing for which experimental results (including flow visualisation) are available [19] and has shown very good agreement even for the case of a 20^{o} bent plate at 20^{o} incidence [22].

Such a tip vortex model is only of practical interest at large angles of attack. For smaller angles the short distance apart of the tip edge vortices dictates very small segment lengths (4.2.3) and hence long computing times.

4.3 Details of the Present Calculations

4.3.1 Geometry

The details of the wing are:

Aspect Ration	4.0
Taper Ratio C_T/C_R	1.0
Flap Chord/c	0.25
Flap Span/b	1.0

Two sweepback angles are considered $\Lambda = 0^{o}$ and 45^{o}

The height of the 0.25s.m.c. above the ground is

$h/b = 0.15$

or $h/c = 0.6$

4.3.2 The vortex model

Figure 5 shows the layout of the quadrilateral vortex rings and wake vortices. In order to keep computing time to a minimum the results are based on 24 surface elements in an 8 (spanwise) by 3 (chordwise) array. (The latter following the two-dimensional results). Ideally more elements should be used; however, the present model should be adequate for demonstrating the essential non-planar effects.

At the tip the vortices are inset by a quarter element width after Rubbert [16].

Each of the trailing vortices has ten straight line segments of length/initial distance apart ratio of 1.3 (except the 3 tip vortices which have an initial ratio of just less than 4 - thus the rate of roll-up at the tip will be relatively slow).

4.3.3 Number of iterations

Each case run (free air or ground effect) includes two iterations, i.e.:

First Iteration:

1) Calculates the vortex distribution for a streamwise vortex wake from the flap trailing edge (WI in Figure 5c)

ii) Calculates lift, drag and centre of pressure with streamwise wake W1

iii) Relaxes vortex wake

Second Iteration:

i) Calculates vortex distribution for the new wake

ii) Relaxes vortex wake - (W2 in Figure 5c)

iii) Calculates lift, etc.

4.4 Discussion of Results

4.4.1 Lift

The overall lift variation with flap deflection is presented in Figure 6 for free air and ground effect conditions, two sweepback angles (0 and 45°) and two vortex wakes (W1, the free streamwise wake, and W2, the wake after the second iteration). Also shown are the C_L curves based on free stream velocity U_∞ and circulation (i.e. $2\Gamma/U_\infty c$). The figure thus presents several points for discussion:

i) Zero Sweepback

a) In free air the basic lift characteristic is linear and shows no difference between the effects of the two vortex wakes. There is only a small difference between actual lift and the $2\Gamma/U_\infty c$ value; the difference varies from zero at $\delta_f = 0^{\circ}$ to about 2% at $\delta_f = 30^{\circ}$ (i.e. the deflected flap and non-planar wake provide a small forward induced velocity even in free air - (2.1.ii))

b) In ground effect the basic lift characteristic is non-linear and shows a small increase in lift from vortex wake W2 compared with W1 (2.3.2). The difference between actual lift and $2\Gamma/U_\infty c$ is here more marked than in free air (2.2.2.b).i)), particularly at the larger flap deflections. ($2\Gamma/U_\infty c$ is 5% higher than actual C_L at $\delta_f = 0^{\circ}$ and 15% higher at $\delta_f = 30^{\circ}$).

c) Comparison of Ground Effect and Free air results

Although there is obviously a substantial increase in circulation with ground effect (2.2.1. i)) throughout the flap deflection range considered, the increase in actual lift above the free air value decreases steadily as the flaps are deflected and eventually goes negative at about $\delta_f = 25^{\circ}$ (2.3.3.)

ii) 45° Sweepback

a) In free air the lift characteristic is non-linear i.e. $\partial C_L / \partial \delta_f$ decreases as δ_f increases. The two vortex wakes give slightly different C_L curves - a difference of 3% at $\delta_f = 30^\circ$. The $2\Gamma/U_\infty c$ curve climbs slowly above the C_L curve (from W2) to a difference of 3% at $\delta_f = 30^\circ$.

b) In ground effect the $C_L \backsim \delta_f$ curve is even more non-linear than in free air and the difference between the curves for wakes W1 and W2 rises to about 5% at $\delta_f = 30^\circ$ (2.3.2). There is an appreciable divergence between the $2\Gamma/U_\infty c$ curve and the C_L curve from W2 as the flaps are deflected, varying from 5% at $\delta_f = 0^\circ$ to 17% at $\delta_f = 30^\circ$.

c) Comparison of Ground Effect with Free air results

The increment in circulation in ground effect, though smaller than that for zero sweepback, is still positive. The actual lift increment - above the free air value - is much smaller than that for zero sweep (possibly the sidewash effect, 2.2.1) combined with the reduced circulation) and goes negative at a smaller flap deflection ($\delta_f = 12^\circ$): by $\delta_f = 30^\circ$ there is a substantial reduction in lift ($\sim$ 10% from the free air value).

The free air flap lift increment is plotted against flap deflection in Figure 7 for two sweepback angles (0° and 45°). At zero sweep the lines for wakes W1 and particularly W2 are in excellent agreement with those from reference 2 but using Quadvort values for $\partial C_L / \partial \alpha$ at $\alpha = 10^\circ$ (note in figure 6 that the Quadvort C_L values at $\alpha = 10^\circ$ lie below those obtained from reference 2). Wake W1 is in fact consistent with the linearised wake basis of the reference 2 lines at small flap deflections. For the 45° sweepback the agreement is good only at small flap deflections. At larger deflections the present calculations (and particularly those for wake W1) fall below the reference 2 line giving a non-linear characteristic.

The ground effect curves are also included in Figure 7 and underline what has already been seen in the two-dimensional case (Figure 2) and what is implied in Figure 6; namely, the substantial loss in flap lifting effectiveness near the ground - particularly at the larger flap deflections. This loss is further evaluated in Figure 8 where the ratio $(\Delta C_{L_f})_g / (\Delta C_{L_f})_\infty$ is plotted against δ_f. The general characteristic is similar to that noted in Figure 1, i.e. a steady reduction in the ratio as surface slope

(in this case flap deflection) increases. At zero sweepback there is a favourable ground effect on flap effectiveness for deflections up to 10^{o} but beyond that ground proximity reduces flap effectiveness. In the swept wing case the ground effect is unfavourable throughout the flap deflection range considered.

The overall lift ratio C_{L_g}/C_{L_∞} is plotted against flap deflection in Figure 9 for the two sweepback angles and for the two wakes. Expressed in this way the non-planar wake effects - i.e. wake W2 results compared with those from wake W1 - are seen to be favourable. The difference at zero sweep is fairly constant over the δ_f range considered, but at 45^{o} sweep the difference varies from zero at $\delta_f = 0^{o}$ to the order of 5% at 30^{o}.

Also shown in Figure 9 are C_{L_g}/C_{L_∞} values obtained from References 1 and 2. The mean value from Reference 1 (which has a $\pm$ 30% tolerance) lies somewhat above the Quadvort result at zero flap deflection particularly for the swept wing. The tolerance includes the Quadvort zero sweep curve at small flap deflections but excludes the whole swept wing curve. The value from Reference 2 (which uses Wieselsberger's[3] method) lies below the Quadvort result for zero sweep but is reasonably close for the swept case (both at zero flap deflection).

4.4.2 Centre of Pressure

The movement of centre of pressure with flap deflection is shown in Figure 10 for the two sweepback cases in free air and in ground effect.

1) Chordwise Position of Centre of Pressure $\bar{\xi}$ (Fig. 10a)

a) Free air

Both sweepback cases have a centre of pressure at 0.24 (of local chord) at zero flap deflection. As flaps are deflected the centre of pressure moves aft - as it should - the zero sweep case moving further aft (0.416 at $\delta_f = 30^{o}$) than the swept case (0.396 at $\delta_f = 30^{o}$) as would be expected from its superior flap lift effectiveness (Figure 7). Only in the swept case at the larger flap deflections is there a plottable difference between the W1 and W2 curves and even then the difference is small.

b) In ground effect

At zero flap deflection the centre of pressure moves rearward (2.2.2 a)) by 0.02 for zero sweep and 0.015 for $\Lambda = 45^{o}$, compared with the free air values. This movement decreases as the flaps are deflected until, at about $\delta_f = 10^{o}$ there is a reversal; beyond this deflection the centre of pressure moves forward in ground effect (2.3.3). The movement is 0.02c at $\delta_f = 30^{o}$ for both sweepback angles.

The difference in the curves for wakes W1 and W2 is again plottable only at the larger flap deflections on the swept wing.

ii) Spanwise Position of Centre of Pressure $\bar{\eta}$ (Fig. 10b)

In all the cases considered the calculated spanwise centre of pressure moves outboard as the flaps are deflected. This tendency will be discussed more fully in connection with the spanwise lift distribution (4.4.5). Apart from this there is a small,changing,effect with sweepback:

a) Zero Sweepback

The variation with flap deflection is linear and the ground effect values with wake W2 tend to be further outboard compared with those in free air. Also the lines for wake W2 tend to be further outboard than those for W1.

b) 45^{o} Sweepback

The starting value for $\bar{\eta}$ at zero flap deflection is further outboard than for the unswept case as it should be (~ 0.465 compared with 0.435). The tendencies as flaps are deflected are reversed in comparison with the unswept case (except for the general outboard movement):the movement is non-linear, the ground effect values tend to be inboard of the free air curves,and the W2 values lie further inboard than those for W1.

4.4.3 Vortex Drag Factor

The vortex drag factor, $k = \pi A C_{D_v} / C_L^{\,2}$, is plotted against flap deflection in Figure 11a for both free air and ground effect and for both sweepback angles. It is noticeable - particularly in the swept wing case - that the calculations predict an increase in k with flap deflection in both free air and ground effect. At first sight

and with linear theory experience, this increase seems very strange since the flaps are full span. However similar increases (shown dotted in Figure 11) are obtained in free air substituting the calculated $\bar{\eta}$ values in Garner's[20] equation:

$$k = 1 + 46.264(\bar{\eta} - 0.42441)^2$$

so it seems possible that the increase in k is partly attributable to the calculated outboard movement of centre of pressure as flaps are deflected.

The increase in k is also partly attributable to the non-linear characteristic in C_L (particularly in the swept case and in ground effect).

The relaxed wake W2 gives a lower k factor than the streamwise wake W1 in both free air and ground effect for the swept wing, but only in ground effect for the unswept wing: the unswept wing in free air has a slightly higher k value with the W2 wake than with W1.

At zero flap deflection the swept and unswept wing have calculated k values remarkably close to each other in free air and in ground effect conditions.

The increments in k arising from ground effect (with wake W2) are presented in Figure 11b for the two sweepback cases, the curves are virtually the same. The increment, which is favourable, reduces slightly with flap deflection. For comparison Δk values from the data sheets[1,2] are also plotted in Figure 11b; that from Reference 2 (based on Wieselsberger's[3] elliptic loading theory) lies very close to the present calculation at $\delta_f = 0$; that from Reference 1 is more optimistic and the present calculations lie outside the quoted tolerance ($\pm$ 30%).

4.4.4 Lift/Vortex Drag Ratio

Figure 12a shows the variation of C_L/C_{D_V} - in effect a measure of the lifting efficiency of the wing - as the flaps are deflected for both free air and ground effect conditions. The efficiency falls considerably in both free air and ground effect as the flaps are deflected. The swept wing appears more efficient than the unswept wing in these terms (i.e. at the same incidence, this would not be the case at the same C_L).

The presence of the ground improves the efficiency over the whole range considered. In relative terms (Figure 12b) the zero sweep wing is 30% more efficient in ground effect (in terms of C_L/C_{D_V} at least) at $\delta_f = 0$ and this figure rises linearly to 38% at $\delta_f = 30^o$. For 45^o sweepback the figure starts near 40% at $\delta_f = 0^o$

rises to 42% at $\delta_f = 20^o$ and then falls back to 41% at $\delta_f = 30^o$.

4.4.5 Spanwise Distribution of Lift

Figure 13 shows the non-dimensional spanwise loading curves for the two sweepback cases. It compares results for free air and ground effect conditions with and without flaps deflected, showing, where plottable, the difference between results from vortex wakes W1 and W2. The C_L value used for non-dimensionalising is that from wake W2

i) Zero Sweep

The main feature is the fuller loading towards the tip with flaps deflected in both free air and ground effect conditions; this has already been implied by the spanwise position of centre of pressure - Figure 10. A possible explanation for this can be gathered from the effect of the tip vortex model used (4.2.4 and Figure 16). In effect an end plate of vorticity has been allowed to form at the tip (Figure 16) and the vorticity vector in this sheet is more or less in the free streamwise direction (possibly slightly below free-streamwise out of ground effect).

When applying the boundary condition of tangential flow over the flap surface the downward component of tip vortex induced velocity - which normally accounts for the rapid fall in loading near the tip - has a decreasing contribution to the normal component as the flap is deflected; to compensate for this the local circulation (i.e. at the flap hinge line in this case) must increase relative to the zero flap condition (i.e. the opposite case to that given in 2.3.1.b) for upwash). The effect is slightly more pronounced in ground effect, particularly with wake W2.

At zero flap deflection there is little difference in the loading shapes for free air and ground effect conditions.

ii) 45^o Sweep

The fuller loading near the tip, which was observed for the zero sweep case with flaps deflected is present here also, though to a lesser extent (particularly in ground effect) - the reduction in this effect possibly arises from the influence of the sidewash velocities (outboard in free air and in ground effect) from the tip edge vortices acting at the swept flap control points (i.e giving an additional downward normal component and hence

tendency to reduce circulation (2.3.1) and also acting at the swept bound vortices giving a reduction in lift (e.g. 2.2.1).

The fall in loading at the root with $\delta_f = 35^o$ has occurred for the swept wing because of the way the flap is deflected. It is in fact a real-flap deflection (accomplished within the program) and because the flap hinge line is swept a small gap appears on the plane of symmetry producing the observed part span effect. This of course contributes to the outboard movement of the centre of pressure (4.4.2) particularly at the larger flap deflections. The difference between the results using wakes W1 and W2 is very marked in this inboard region.

At zero flap deflection there is little difference between free air and ground effect loading shapes.

4.4.6 Spanwise Locus of $\bar{\xi}$

The locus of $\bar{\xi}$ for the two sweep back cases is shown in Figure 14. Results for free air and ground effect conditions with flaps at 0^o and 30^o are presented.

i) Zero Sweep

At zero flap deflection the rearward shift in $\bar{\xi}$ with ground effect (already seen in Figure 10a) is seen to be evenly distributed over the span for wake W2; at the tip the rearward shift given by wake W1 is smaller. Generally, towards the tip, $\bar{\xi}$ moves slightly forward except very near the tip where it tends to move rearward again particularly in ground effect.

With the flap deflected the most striking feature (apart from the expected general rearward movement) is the large rearward movement near the tip, this would seem to underline the hypothesis concerning the effect of the tip edge vortices (4.4.5.i) since the hinge line vortex (at 0.75c) would be the one most likely to carry the increase in circulation.

The reversal in the movement of $\bar{\xi}$ in ground effect as the flap is deflected has already been noted in Figure 10a; it is seen here to occur mainly inboard from the tip.

ii) 45^o Sweep

At zero flap deflection the shape is seen to be very conventional (for a swept wing) in both free air and ground effect conditions. The ground

effect with wake W2 again gives a fairly uniform rearward shift; with wake W1 however, a smaller rearward shift is given over the outer part of the wing.

With the flap deflected the locus is completely changed; apart from its expected rearward movement, the locus at the root is affected by the part span effect previously noted (4.4.5 ii) giving a reduced rearward shift there, and at the tip the rearward shift already discussed for the unswept wing is again present though to a lesser extent. The rearward shift is also obscured by the natural forward movement in the tip region with zero flap deflection.

The reversal in trend of ground effect on $\bar{\xi}$ with flap deflection (see also Figure 10a) is seen to be mainly concentrated in the mid-semi-span region. The difference between the W1 and W2 results in the inboard region with flaps deflected indicates that the relative loss in lift there for wake W1 (Figure 13) occurs mainly over the rear part of the wing.

4.4.7 Spanwise Distribution of Vortex Drag

i) Zero Sweep

Figure 15a shows the spanwise variation of Cd_V/C_L^2 for zero and 30^o flap deflections in and out of ground effect.

The zero flap free air curve is in fair agreement with Garner's[20] curve. The reduction in vortex drag in ground effect occurs mainly near the root (since it depends primarily on image trailing vortex upwash (2.2.1)).

With flap deflected in free air there is a reduction in Cd_V/C_L^2 over two thirds of the span (possibly an effect from the non-planar wake, e.g. 2.3.2) but there is a sharp increase near the tip (possibly the combination of the strong downwash and strong circulation there (4.4.5 i)). Similar trends can be seen in the ground effect curve.

ii) 45^o Sweep

The swept wing curves are shown in Figure 15b. Again the calculated result for the zero flap free air case shows fair agreement with Garner's[20] curve though it indicates a much smoother variation across the span. The reduction in vortex drag with ground effect is seen to occur mainly in the mid semispan region.

With flap deflected there is again a rise in vortex drag outboard though this is obscured to a certain extent by the natural rapid fall in vortex drag there for the zero flap case. In ground effect the main part of the vortex drag reduction occurs around the 0.75 semi-span region.

4.4.8 Typical Vortex Wake Shape

Finally, in Figure 16, a typical vortex wake shape is shown (after the second iteration). The wake is for the unswept wing with 30^{o} flap in ground effect.

Note the fairly rapid outward movement of the vortices as they approach the ground plane and the general outward movement of the tip vorticity (hence the rear view is oblique to the 'helical' roll up of the tip vortices)

In rolling round the centroid of tip vorticity the leading edge tip vortex can be seen to first move inboard then downwards, parallel to the deflected flap, while the hinge line tip vortex first moves more or less parallel to the chord plane (outboard) then upwards: similar tendencies can be observed in the flow visualisation studies in reference 19.

5.0 CONCLUSIONS

These calculations demonstrate the practical importance of including the influence of camber, incidence and non-planar wake in the evaluation of ground effect on aerodynamic characteristics at small ground heights : otherwise the calculated changes from free air conditions can be too optimistic and in some cases even of the wrong sign.

The main features shown by these calculations are:-

a) At constant incidence a wing (and in particular a swept wing) with large camber can actually lose lift near the ground (whereas existing methods generally give an increase in lift).

b) The reduction in vortex drag near the ground is generally smaller than that given by existing methods (and according to the model used here applies to a higher basic vortex drag at large flap deflections).

c) The rearward movement of centre of pressure with ground effect, which applies at small incidence and camber, can change to a forward movement for wings with large camber.

d) Ground effect calculations based on a free streamwise planar wake from the flap trailing edge are more pessimistic in terms of lift and vortex drag in comparison with those based on a relaxed wake.

The multi-vortex method is a powerful tool for evaluating the ground effect on lift, centre of pressure and pressure distribution in two dimensional potential flow over a wide range of incidence, camber and height above ground.

A simple one-vortex theory is adequate (compared with the multi-vortex method) for representing the lift effect on a flat plate in two-dimensional potential flow down to ground heights of the order of half a chord, but is not satisfactory for dealing with camber.

The Quadvort method with vortex-wake relaxation promises to be a powerful tool for dealing with complicated three-dimensional flow interference problems of this type. Clearly, however, further work is required in order to correlate the potential flow calculations with real flow problems.

REFERENCES

1. Engineering Sciences Data
Aerodynamics Sub-Series Volume 3
Aircraft 01.01.01

2. U.S.A.F. Stability and Control Handbook

3. C. Wieselsberger "Uber den Flügelwiderstand in der Nähe der Bodens"
Zeitschrift für Flügtechnik, Vol. 12 No. 145, 1921.
(see also "Wing Resistance Near the Ground"
NACA TM No. 77, 1922).

4. F. Thomas 'Aerodynamic Properties of Sweptback and Delta
Wings Near the Ground'
R.A.E. Library Translation No. 882, March 1960.

5. I. Tani
M. Taima
S. Simidu
'The Effect of Ground on the Aerodynamic Characteristics of a Monoplane Wing'
Rep. No. 156, Aero.Res.Inst., Tokyo Imp.Univ., 1937.

6. G.H. Saunders 'Aerodynamic Characteristics of Wings in Ground
Proximity'
Canadian Aero. & Space Journal, Volume II, No. 6,
June 1965.

7. T.P. Kalman
W.P. Rodden
J.P. Giesing
'Application of the Doublet-Lattice Method to Non-Planar
Configurations in Subsonic Flow'
Journal of Aircraft, Vol. 8, No. 6, June 1971.

8. S. Tomotika
K. Tamada
H. Umemoto
'The Lift and Moment Acting on a Circular-Arc
Aerofoil in a Stream Bounded by a Plane Wall'
Quart. Journal Mech. & Applied Maths 4, 122, (1950).

9. P.E. Rubbert 'Two-Dimensional Airfoils in Ground Effect'
Boeing Document D6-8117, 1962.

10. D.J. Butter
G.J. Hancock
'A Numerical Method for Calculating The Trailing
Vortex System Behind a Swept Wing at Low Speed'
Journal of the Royal Aeronautical Soc., Vol. 75,
No. 728, August 1971.

11. S.M. Belotserkovskii 'Calculation of the Flow About Wings of Arbitrary
Planform at a Wide Range of Angles of Attack'
R.A.E. Library Translation No. 1433, 1970.

12 J.E. Hackett, M.R. Evans — 'Vortex Wakes Behind High-Lift Wings' Journal of Aircraft, Vol. 8, No. 5, May 1971.

13. B. Maskew — 'Calculation of the Three-Dimensional Potential Flow Around Lifting Non-Planar Wings and Wing Bodies Using a Surface Distribution of Quadrilateral Vortex Rings' Loughborough University of Technology Report TT 7009, 1970.

14. S.M. Belotserkovskii — 'The Theory of Thin Wings in Subsonic Flow' Plenum Press, New York, 1967.

15. S.G. Hedman — 'Vortex Lattice Method for Calculation of Quasi Steady State Loadings of Thin Elastic Wings in Subsonic Flow' F.F.A. Report 105, 1965.

16. P.E. Rubbert — 'Theoretical Characteristics of Arbitrary Wings by a Non-Planar Vortex Lattice Method' Boeing Co. Report D6-9244, 1964.

17. S. Tomotika — 'Further Studies on the Effect of the Ground Upon Lift of a Monoplane Aerofoil' Aeronautical Research Institute, Tokyo Imperial University, Report No. 120 (1935).

18. S.D. Ermolenko — 'On the Non-Linear Theory of Wings of Small Aspect Ratio' R.A.E. Library Translation No. 1218 (1967)

19. R.H. Wickens — 'The Vortex Wake and Aerodynamic Load Distribution of Slender Rectangular Wings' Canadian Aeronautics & Space Journal, Vol. 13, No. 6, June 1967.

20. H.C. Garner — 'Some Remarks on Vortex Drag and Its Spanwise Distribution in Incompressible Flow' Journal of the Royal Aeronautical Society July 1968.

21. R.M. Licher — 'Increase in lift for two and three dimensional wings near the ground'. Douglas Report No. SM-22615 Oct. 1956.

22. B. Maskew — 'Numerical Lifting Surface Methods for calculating the potential flow about wings and wing-bodies of arbitrary geometry' Ph.D. Thesis, Loughborough University of Technology, Oct. 1972

APPENDIX

The Ground Effect on the Flat Plate at Incidence in Two-Dimensional Flow

Consider the single vortex representation of the flat plate in free air conditions: the vortex is placed at the 0.25c point and the boundary condition of tangential flow is satisfied at the 0.75c point.

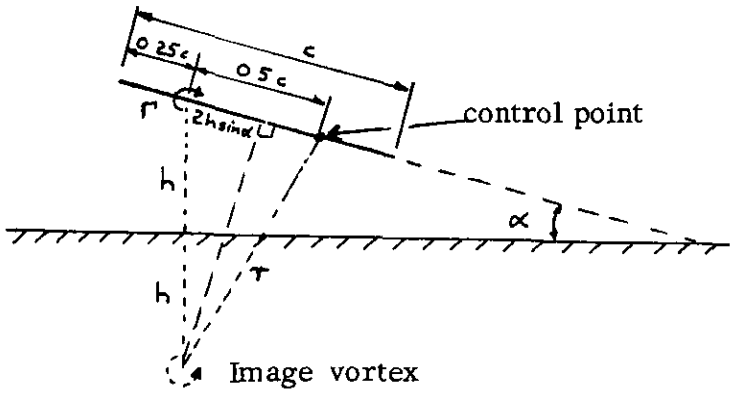

First consider the free air calculation:

The *downwash induced at the control point by the vortex is* $\Gamma/(2\pi c/2)$ *and this* must cancel the upward component of free stream velocity, i.e. $U_\infty \sin\alpha$

Thus $\Gamma = \pi c U_\infty \sin\alpha$

The velocity acting at the vortex is U_∞

Thus

Lift = $\rho U_\infty \Gamma$ /unit span

and C_{ℓ_∞} = Lift/$\frac{1}{2}\rho U_\infty^2 c$

i.e. $C_{\ell_\infty} = 2\pi \sin\alpha$

In ground effect the image vortex has two effects:

i) it modifies the boundary condition equation

ii) it modifies the local velocity at the vortex.

Consider i):

The additional normal component of induced velocity is an upwash of magnitude;

$$\frac{\Gamma_g}{2\pi r^2}\left(\frac{c}{2} - 2h\sin\alpha\right)$$

where $r^2 = 4h^2 + \left(\frac{c}{2}\right)^2 - 2hc\sin\alpha$

Γ_g = the circulation in ground effect.

Thus the boundary condition equation in ground effect becomes:

$$\frac{\Gamma_g}{2\pi}\left\{\frac{1}{c/2} - \frac{\frac{c}{2} - 2h\sin\alpha}{4h^2 + \left(\frac{c}{2}\right)^2 - 2hc\sin\alpha}\right\} = U_\infty \sin\alpha$$

i.e.

$$\frac{\Gamma_g}{2\pi}\left\{\frac{2\left\{4h^2 + \left(\frac{c}{2}\right)^2 - 2hc\sin\alpha\right\} - \frac{c}{2}^2 + 2hc\sin\alpha}{c\left\{4h^2 + \left(\frac{c}{2}\right)^2 - 2hc\sin\alpha\right\}}\right\} = U_\infty \sin\alpha$$

i.e.

$$\frac{\Gamma_g}{\pi}\left\{4h^2 - hc\sin\alpha\right\} = U_\infty c\sin\alpha\left\{4h^2 - 2hc\sin\alpha + \left(\frac{c}{2}\right)^2\right\}$$

i.e.

$$\Gamma_g = \pi c U_\infty \sin\alpha\left\{1 + \frac{\left(\frac{c}{2}\right)^2 - hc\sin\alpha}{4h^2 - hc\sin\alpha}\right\}$$

or

$$\frac{\Gamma_g}{\Gamma_\infty} = F$$

where $F = 1 + \left\{\frac{\left(\frac{c}{2}\right)^2 - hc\sin\alpha}{4h^2 - hc\sin\alpha}\right\} = 1 + \left\{\frac{\frac{1}{4} - \frac{h}{c}\sin\alpha}{4\left(\frac{h}{c}\right)^2 - \frac{h}{c}\sin\alpha}\right\}$

Consider next condition ii):

The local velocity at the vortex becomes:

$$U_g = U_\infty - \frac{\Gamma_g}{4\pi h}$$

i.e.

$$U_g = U_\infty\left\{1 - \frac{F}{4}\frac{c}{h}\sin\alpha\right\}$$

Lift = $\rho U_g \Gamma_g$ /unit span

$$= \rho U_\infty\left\{1 - \frac{F}{4}\frac{c}{h}\sin\alpha\right\} F\pi c U_\infty \sin\alpha$$

Thus $C_{\ell_g} = \dfrac{F\rho U_\infty^2 \pi c\sin\alpha\left\{1 - \frac{F}{4}\frac{c}{h}\sin\alpha\right\}}{\frac{1}{2}\rho U_\infty^2 c}$

i.e. $$C_{\ell_g} = 2\pi \sin\alpha F \left\{ 1 - \frac{F}{4} \frac{c}{h} \sin\alpha \right\}$$

or $$\frac{C_{\ell_g}}{C_{\ell_\infty}} = F \left\{ 1 - \frac{F}{8\pi} \frac{c}{h} C_{\ell_\infty} \right\}$$

LIST OF SYMBOLS

c	wing chord
c_f	flap chord
b	wing span
A	aspect ratio = b/c
Λ	sweepback angle
h	height of aerofoil 0.25 standard mean chord above the ground plane (except in case of 2-D circular arc aerofoil where h is height of 0.5c point (see Figure 2))
ξ	chordwise distance from local leading edge (non-dimensionalised by c)
η	spanwise distance from plane of symmetry (non-dimensionalised by b/2)
$\bar{\xi}$	chordwise position of centre of pressure
$\bar{\eta}$	spanwise position of centre of pressure on half the wing
α	incidence
δ_f	flap deflection angle (in vertical streamwise plane)
ρ	air density
U	velocity
C_p	pressure coefficient
Γ	circulation
F	ratio of circulation in ground effect to that in free air, i.e. Γ_g / Γ_∞
C_ℓ	section lift coefficient
C_m	section moment coefficient
C_{d_V}	section vortex drag coefficient
C_L	overall lift coefficient
C_{D_V}	overall vortex drag coefficient
k	vortex drag factor = $\pi A\, C_{D_V}/C_L^{\,2}$
ΔC_{L_f}	increment in lift coefficient from deflected flap

Subscripts

∞	in free air
g	in ground effect

LIST OF TABLES AND FIGURES

TABLE 1

Static Ground Heights of Various Aircraft

	h/c	h/b
Trident	0.33	0.08
Nimrod	0.46	0.05
A300B Airbus	0.60	0.08
Buccaneer	0.62	0.16
Phantom	0.36	0.13
Mirage	0.34	0.18

TABLE 2

Lift and Centre of Pressure in Two-Dimensional Flow

Comparison of 3 and 27 Vortex Results from Multi-Vortex Method

$h/c = 0.6$

$\alpha = 10^{o}$

$c_f/c = 0.25$

Flap Deflection	Conditions	Number of Vortices	C_ℓ	$\bar{\xi}$
0^{o}	Free air	27	1.091	0.2500
		3	1.091	0.2500
	Ground Effect	27	1.099	0.2697
		3	1.102	0.2680
30^{o}	Free air	27	2.940	0.3531
		3	2.983	0.3557
	Ground Effect	27	2.214	0.3540
		3	2.238	0.3559

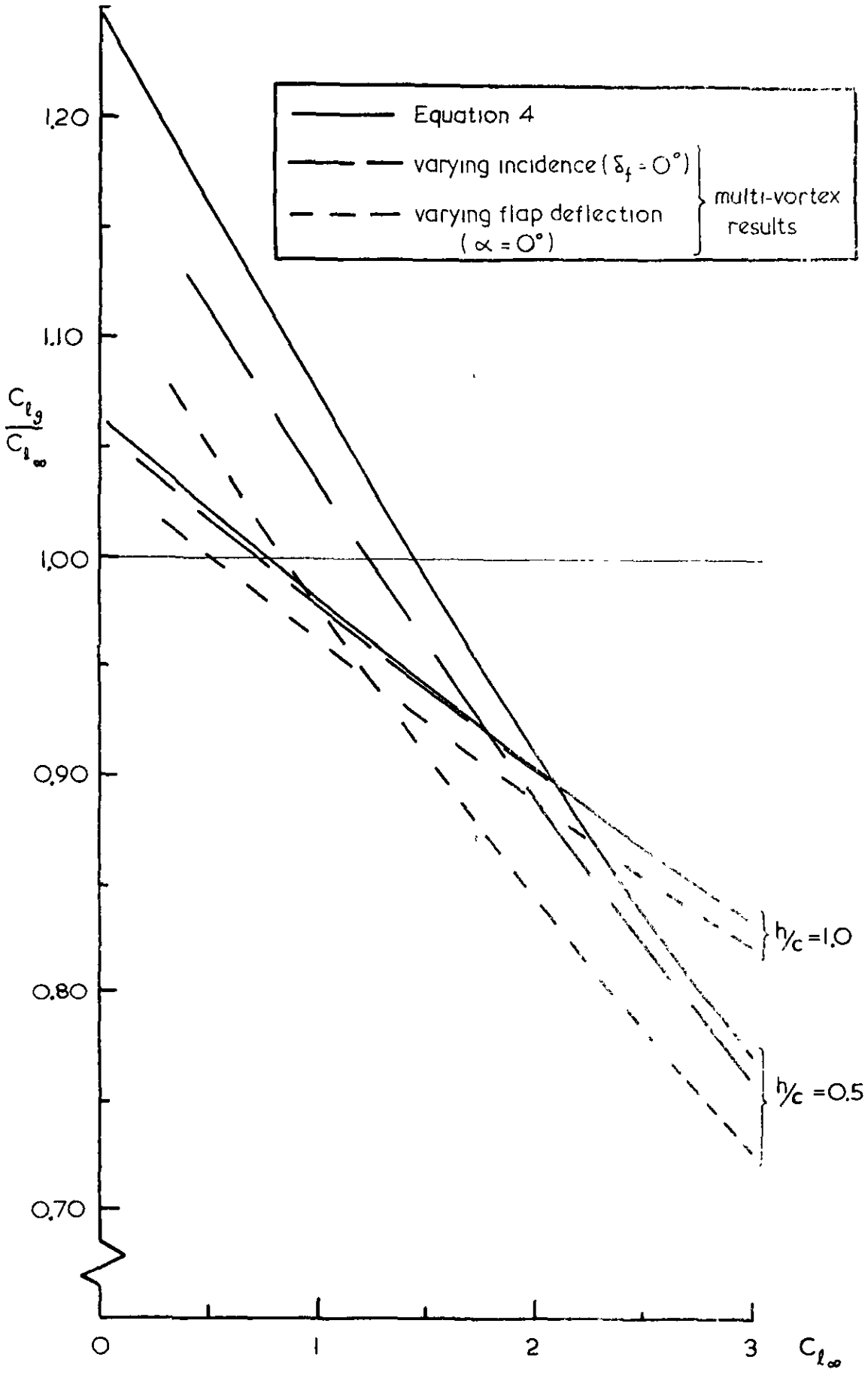

a) Ratio of C_{l_g}/C_{l_∞} as a function of C_{l_∞} for two ground heights.

Figure 1 CALCULATED EFFECT OF GROUND PROXIMITY ON LIFT IN TWO-DIMENSIONAL FLOW.

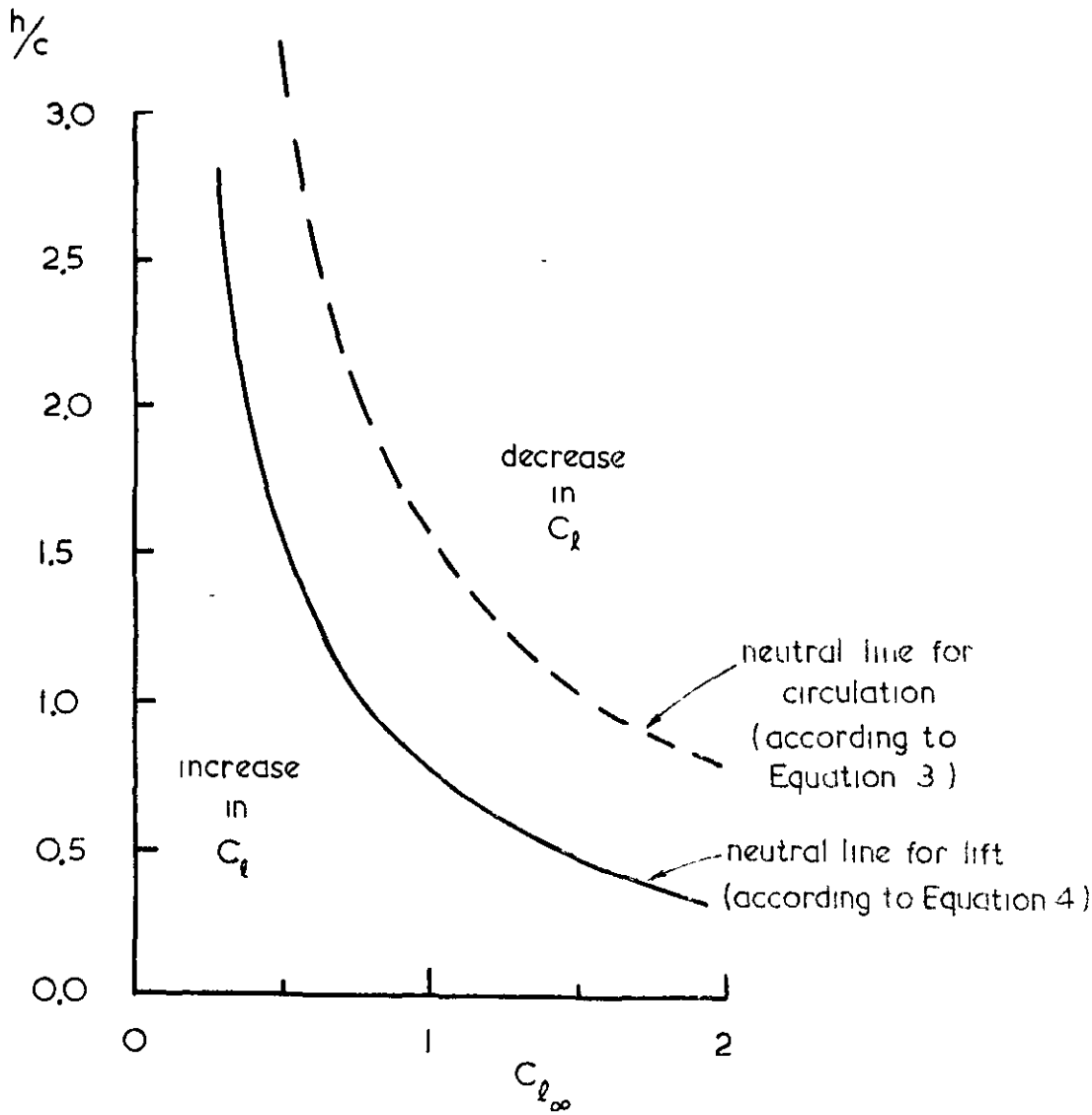

b) **Ground height for neutral lift effect according to single vortex theory.**

Figure 1 CONCLUDED

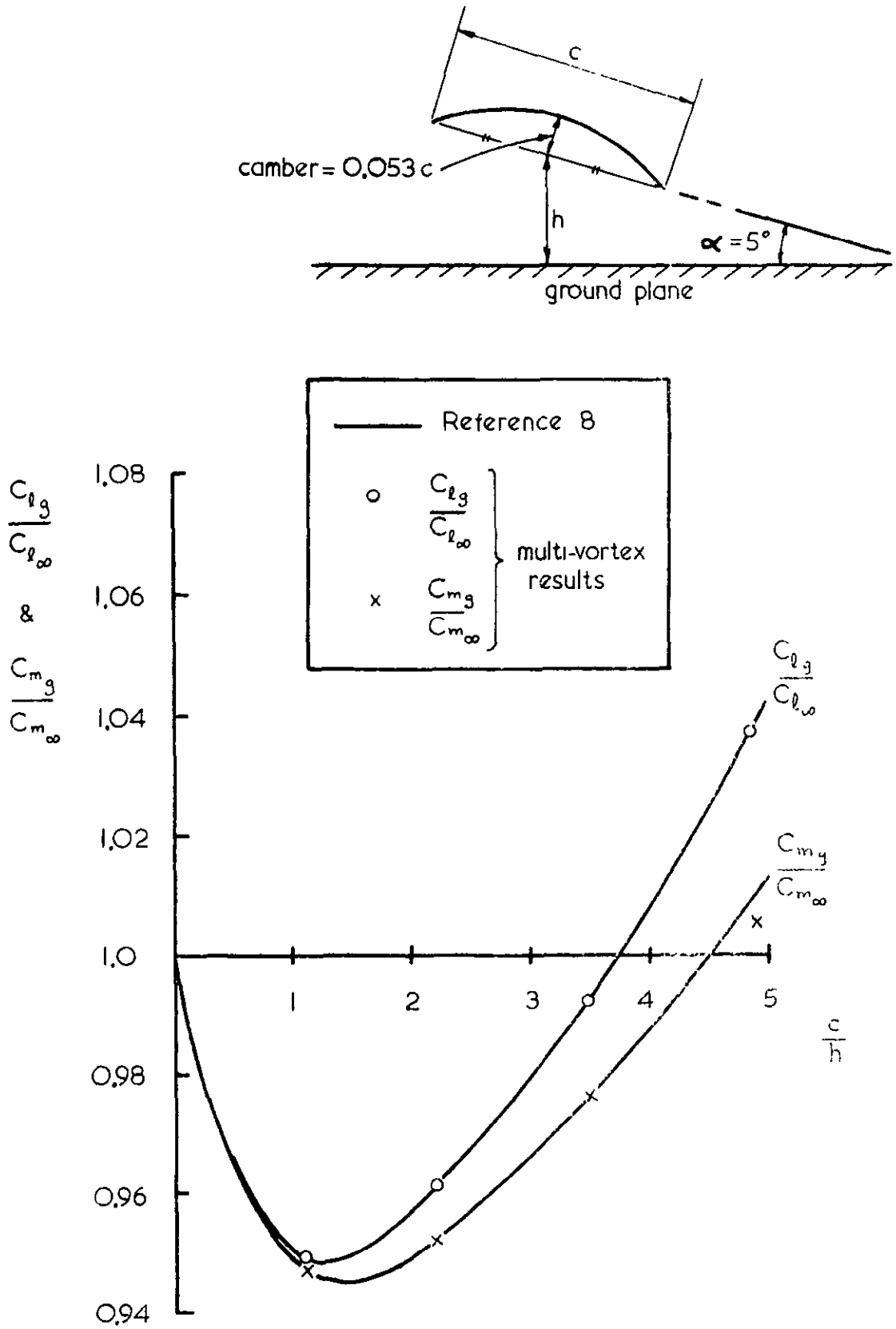

Figure 2 COMPARISON OF CALCULATED LIFT AND MOMENT RESULTS FOR A CIRCULAR-ARC WING IN TWO-DIMENSIONAL FLOW.

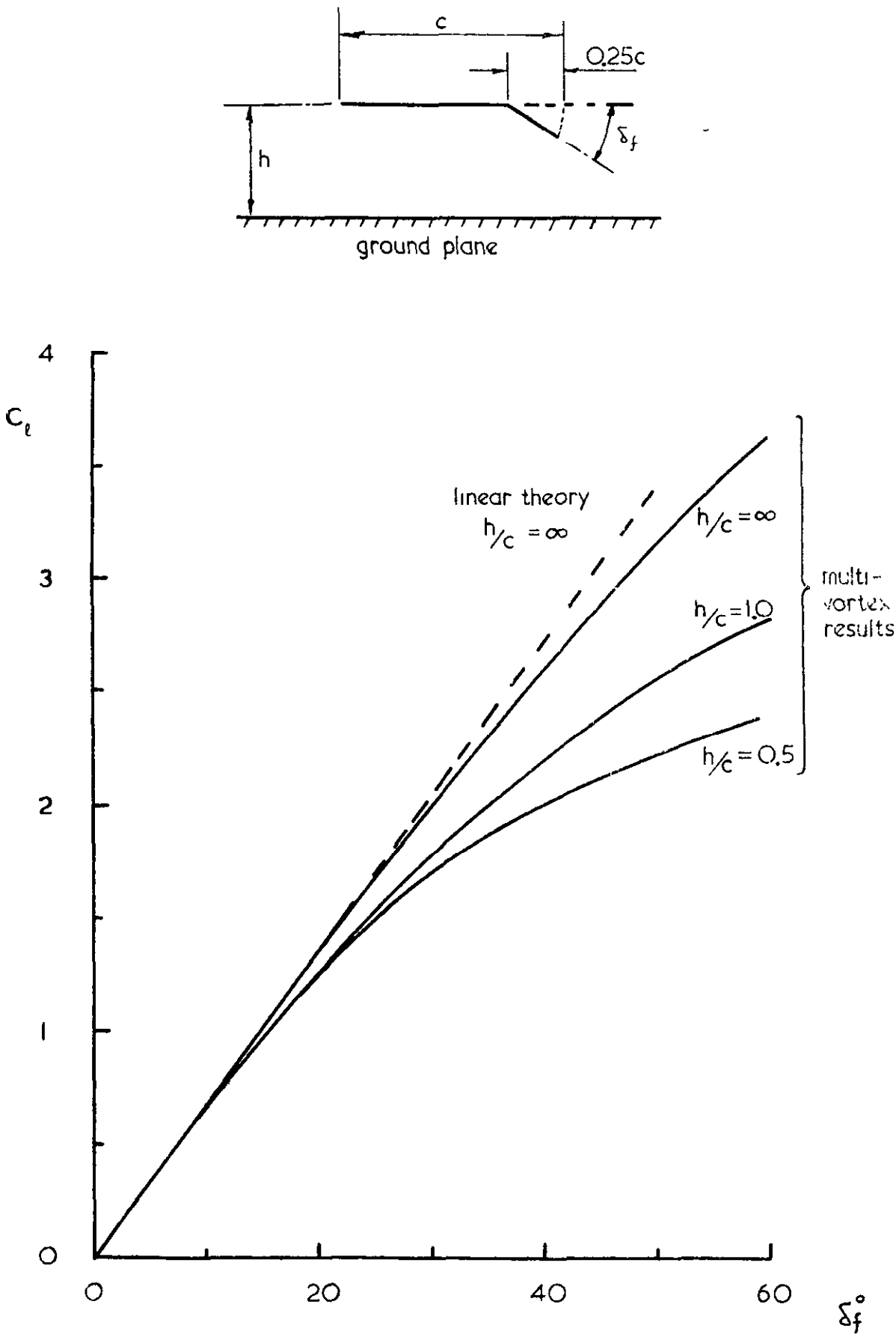

Figure 3 VARIATION IN LIFT WITH FLAP DEFLECTION AT VARIOUS GROUND HEIGHTS ACCORDING TO THE TWO-DIMENSIONAL MULTI-VORTEX METHOD.

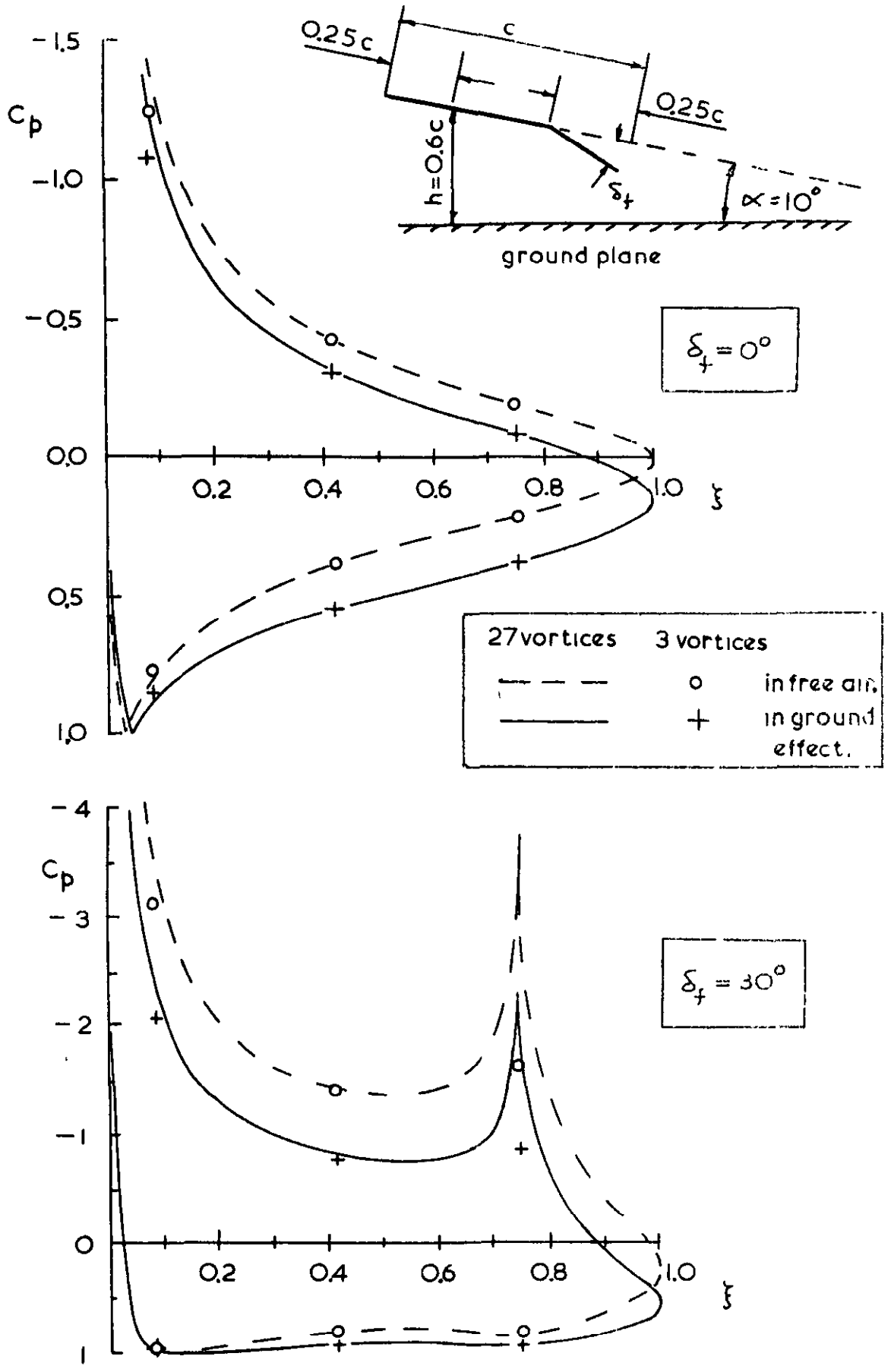

Figure 4 COMPARISON OF PRESSURE DISTRIBUTIONS FROM MULTI-VORTEX METHOD USING 3 AND 27 VORTICES.

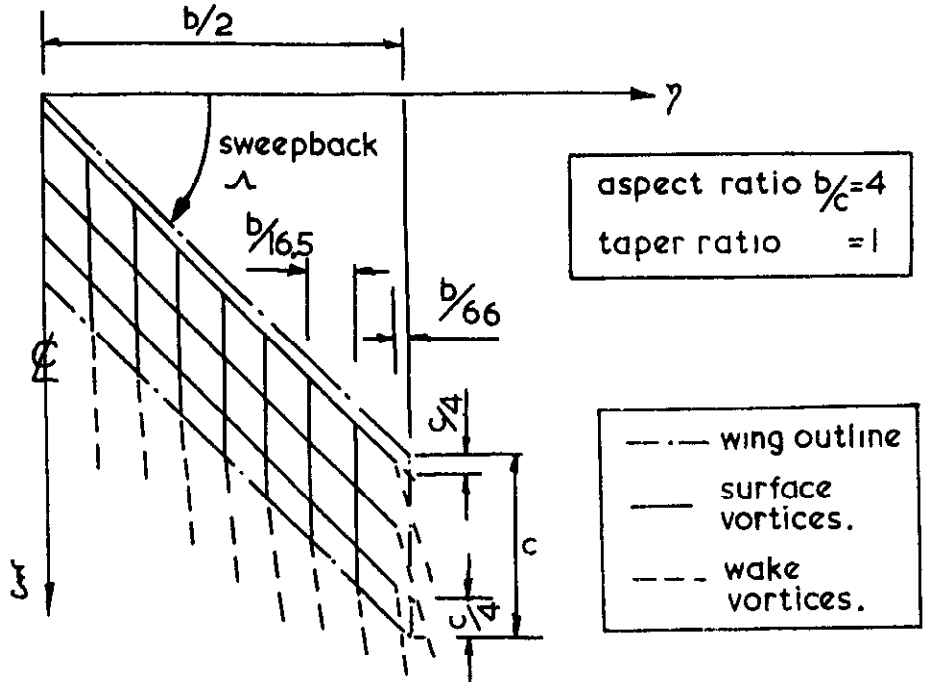

a) Layout of quadrilateral vortex rings and trailing vortices.

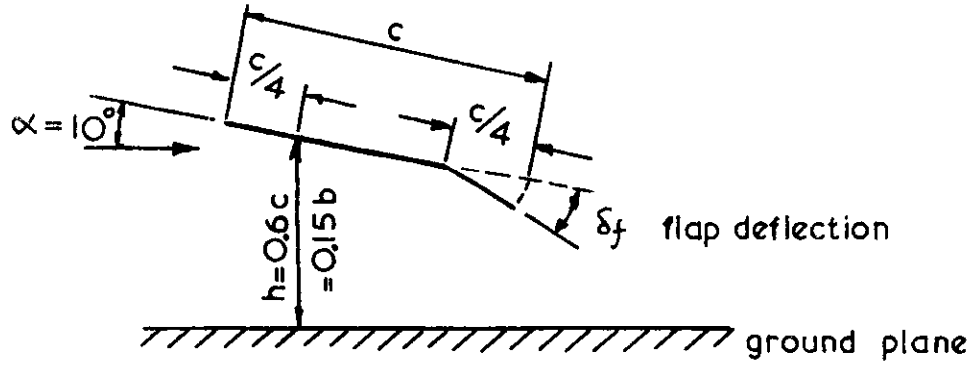

b) Geometry of the section at the standard mean chord in relation to the ground plane.

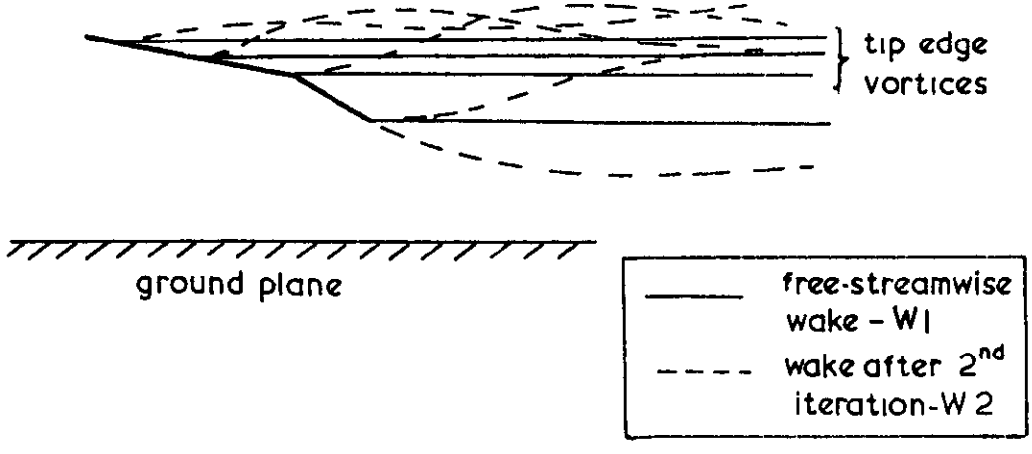

c) Illustration of vortex wakes W1 and W2.

Figure 5 WING AND VORTEX-WAKE DATA FOR FIGURES 6 TO 16.

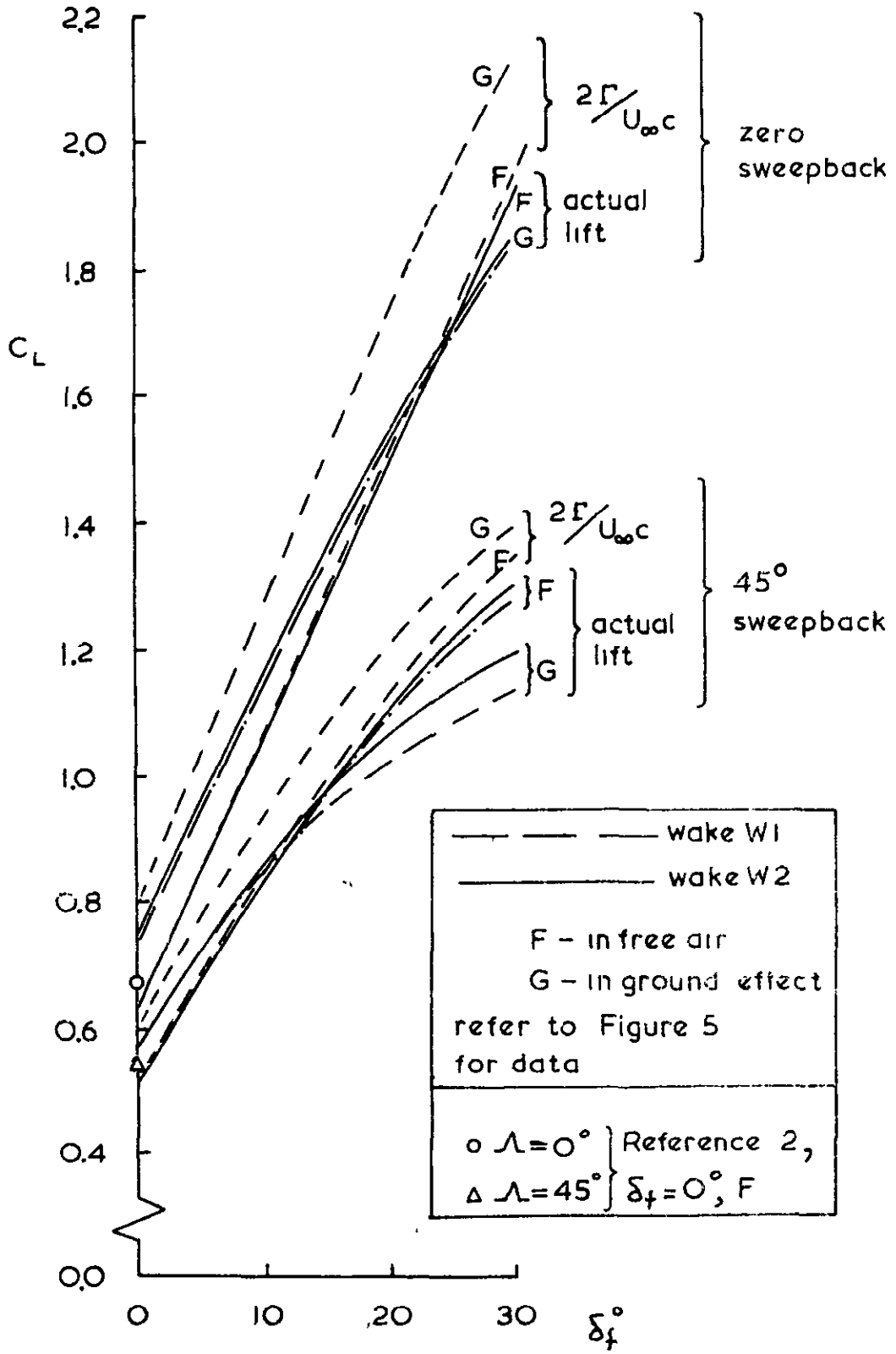

Figure 6 CALCULATED VARIATION OF OVERALL LIFT WITH FLAP DEFLECTION.

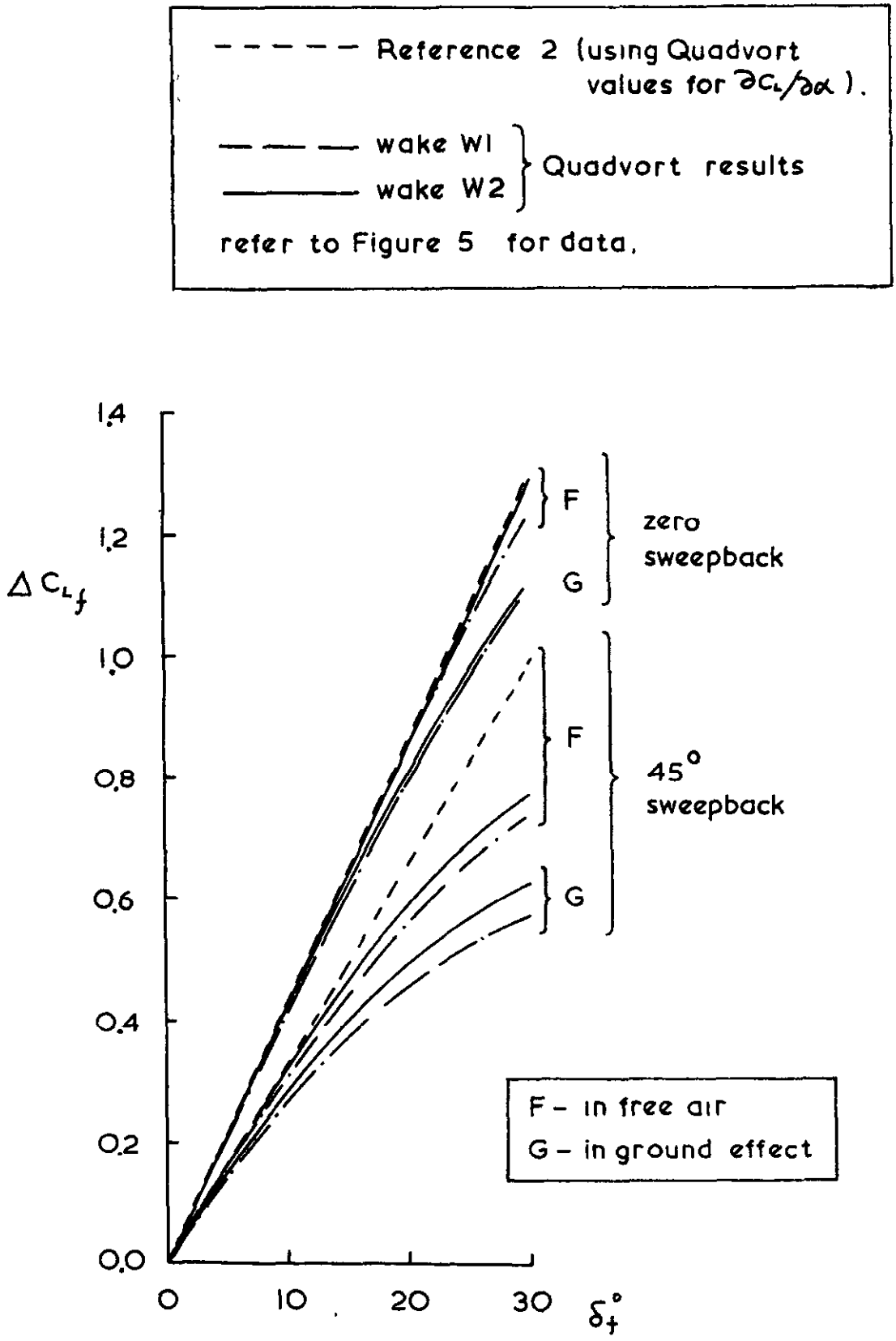

Figure 7 CALCULATED VARIATION OF FLAP LIFT INCREMENT WITH FLAP DEFLECTION.

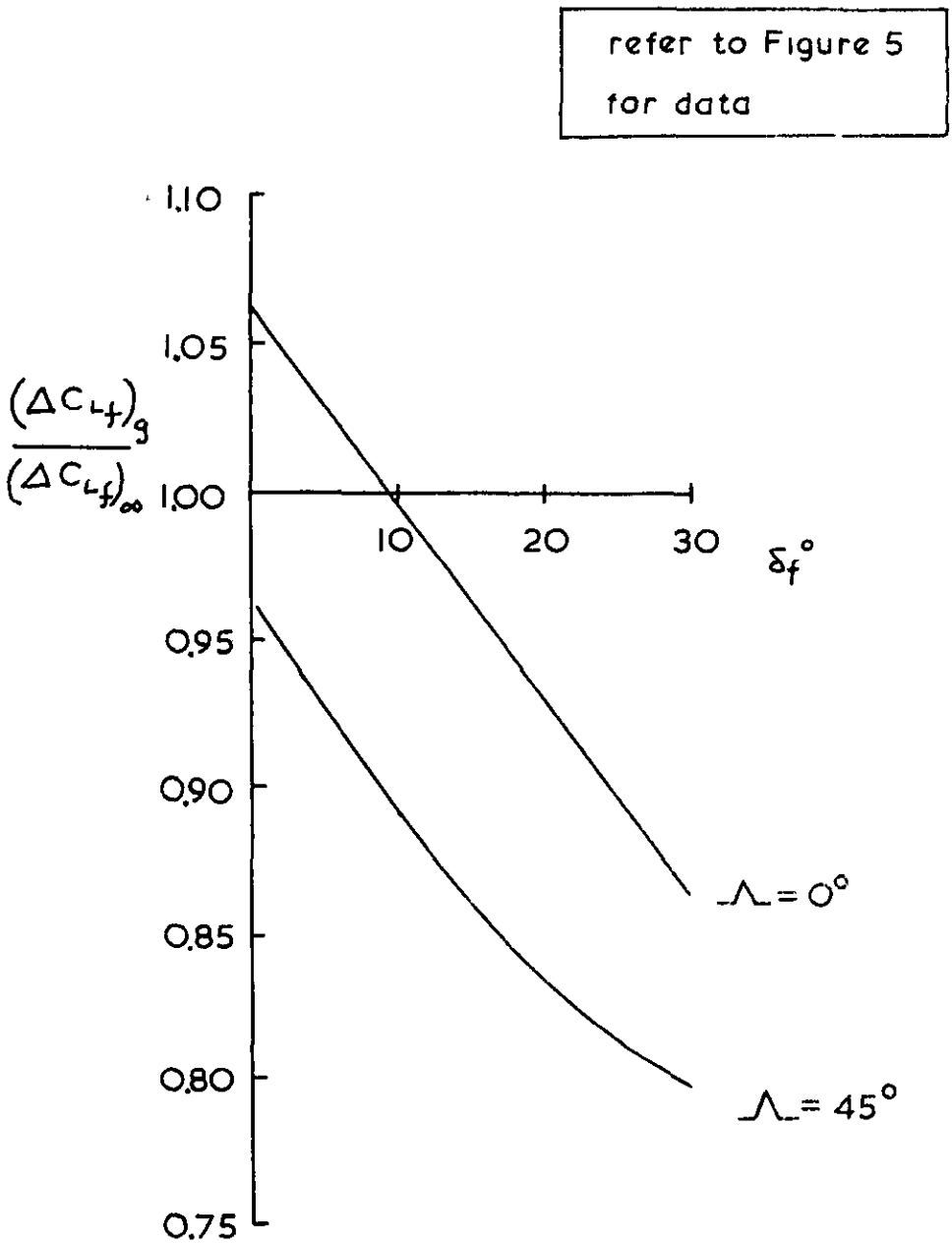

Figure 8 CALCULATED RATIO OF FLAP LIFT INCREMENT IN GROUND EFFECT TO THAT IN FREE AIR AS A FUNCTION OF FLAP DEFLECTION.

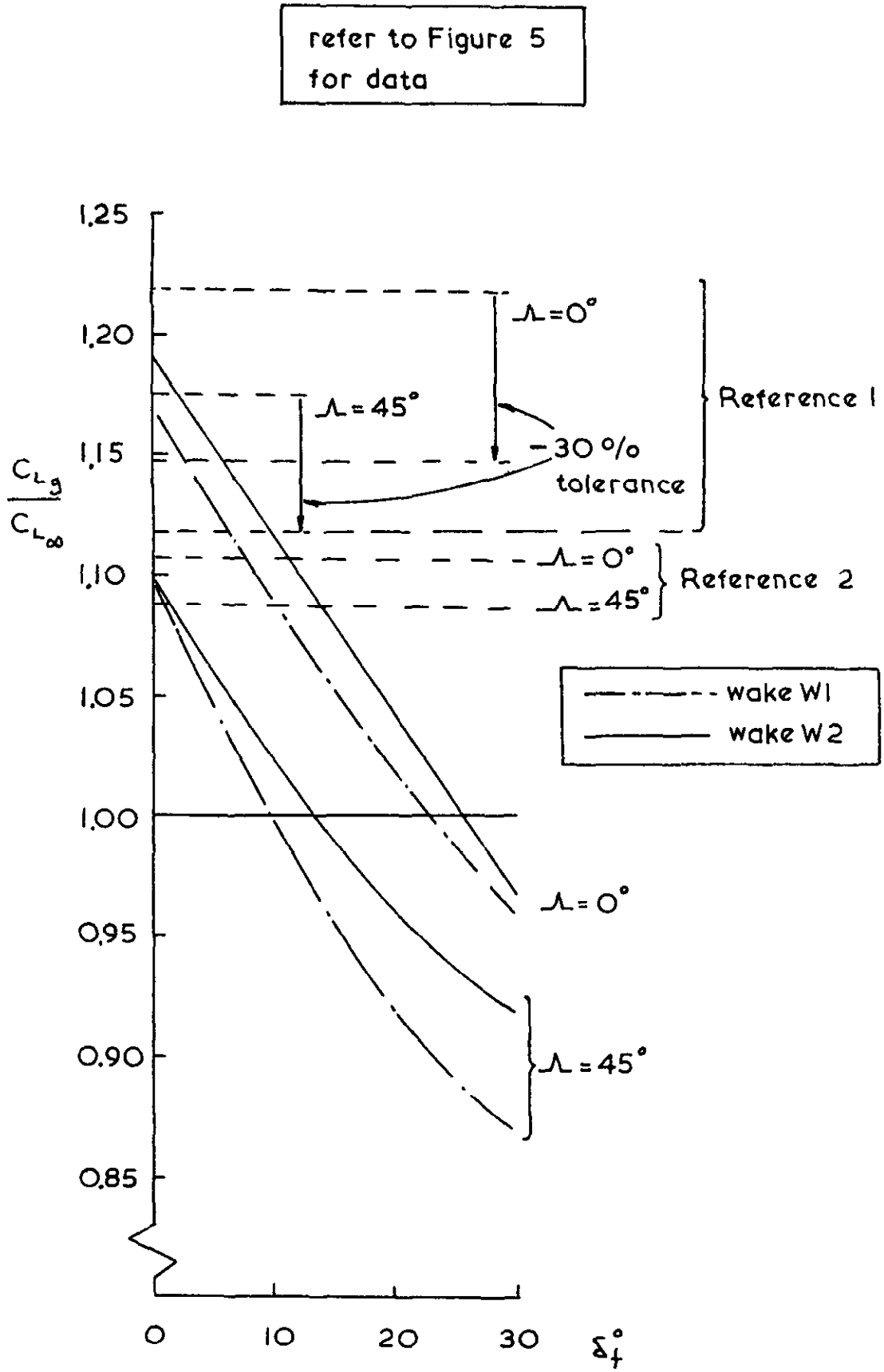

Figure 9 CALCULATED RATIO OF OVERALL LIFT IN GROUND EFFECT TO THAT IN FREE AIR AS A FUNCTION OF FLAP DEFLECTION.

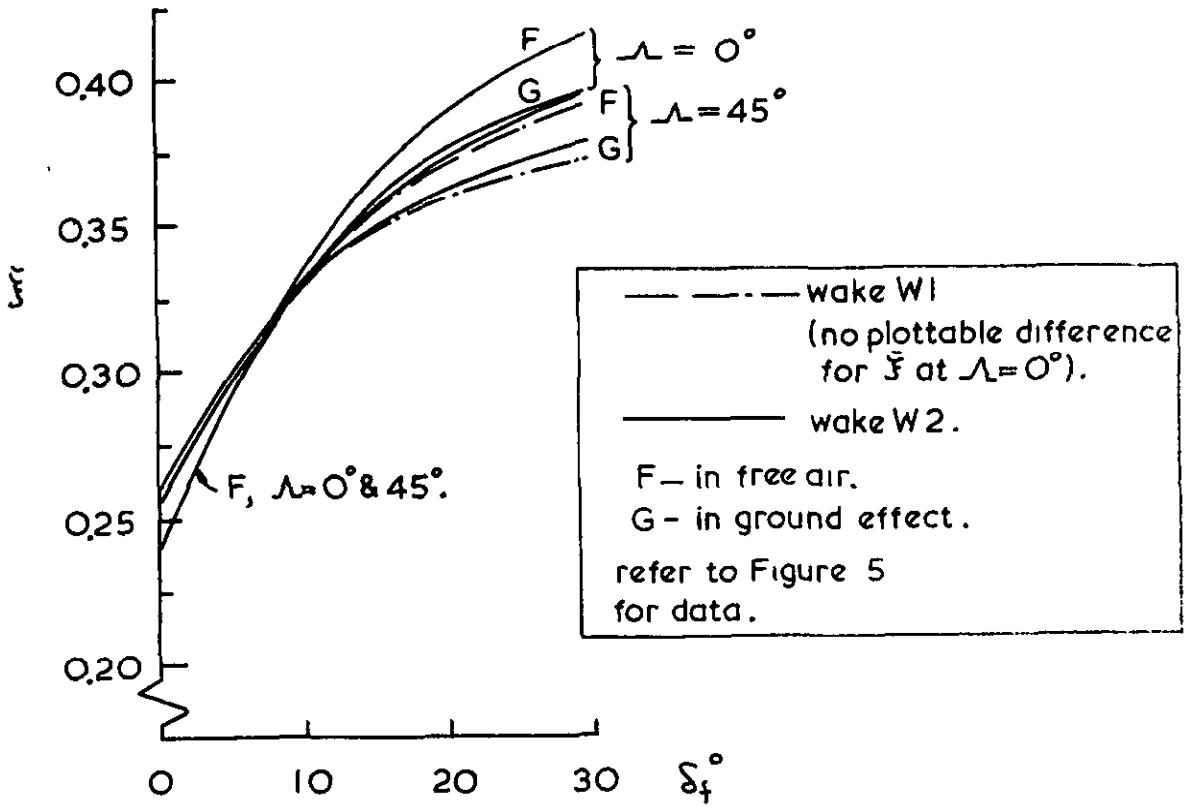

a) Chordwise Position

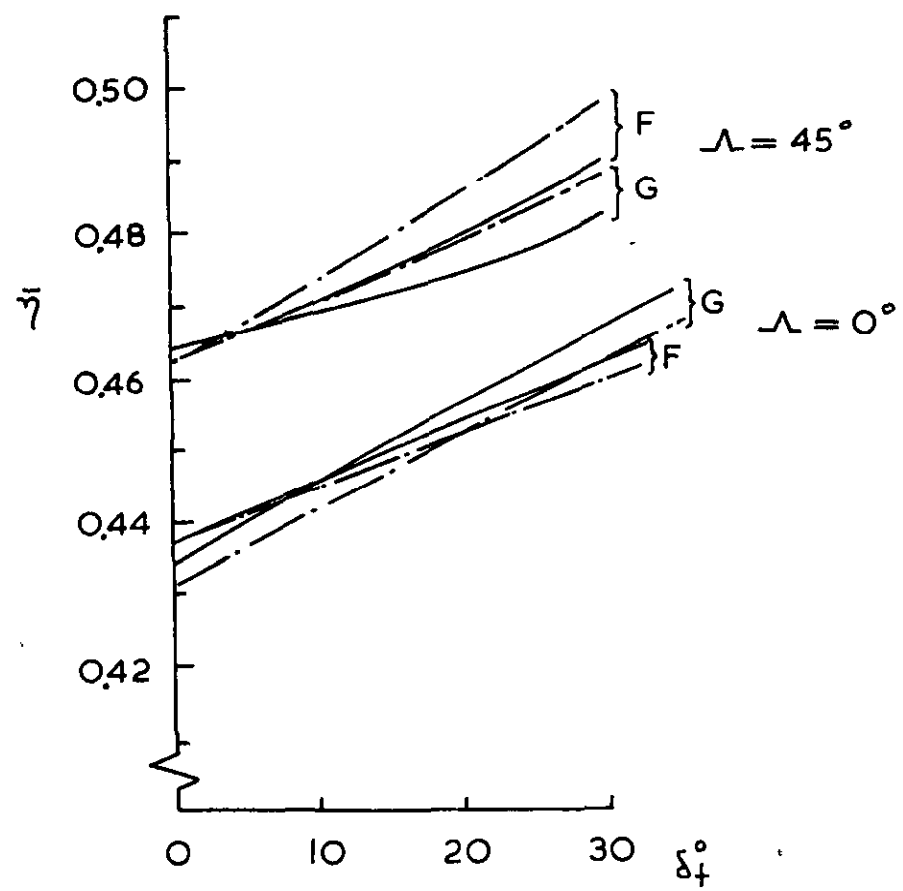

b) Spanwise Position

Figure 10 CALCULATED MOVEMENT OF CENTRE OF PRESSURE POSITION WITH FLAP DEFLECTION.

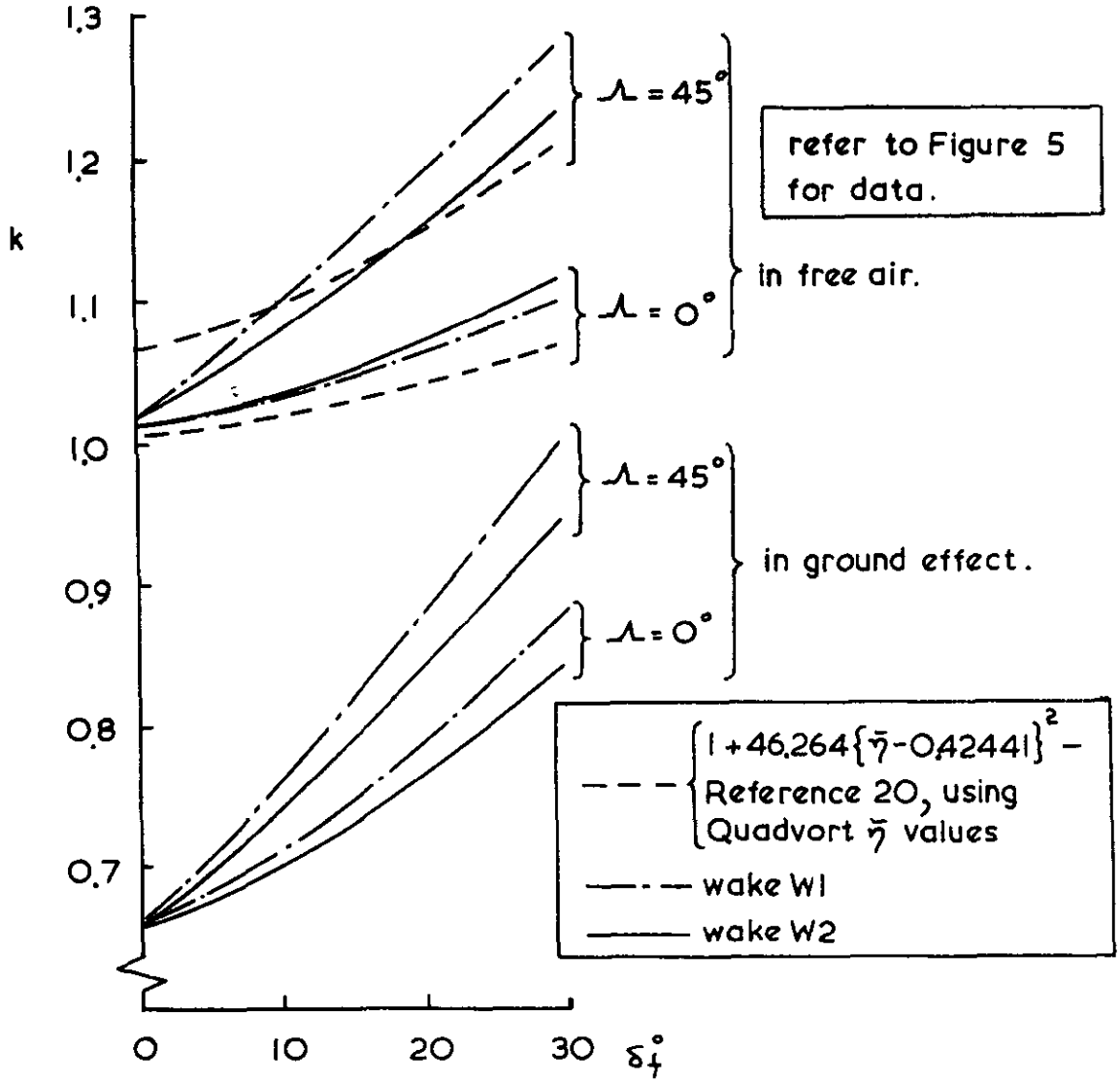

a) Variation of vortex drag factor with flap deflection in free air and in ground effect.

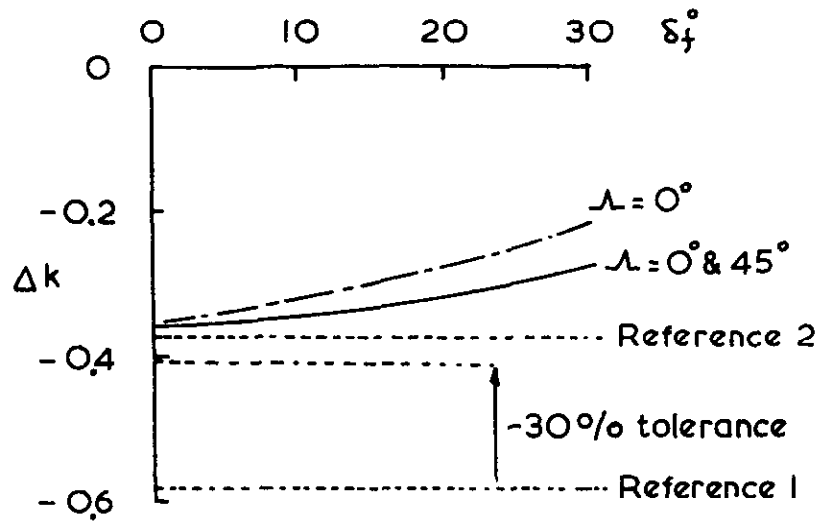

b) Increment in vortex drag factor from ground effect.

Figure 11 CALCULATED VORTEX DRAG FACTOR CHARACTERISTICS.

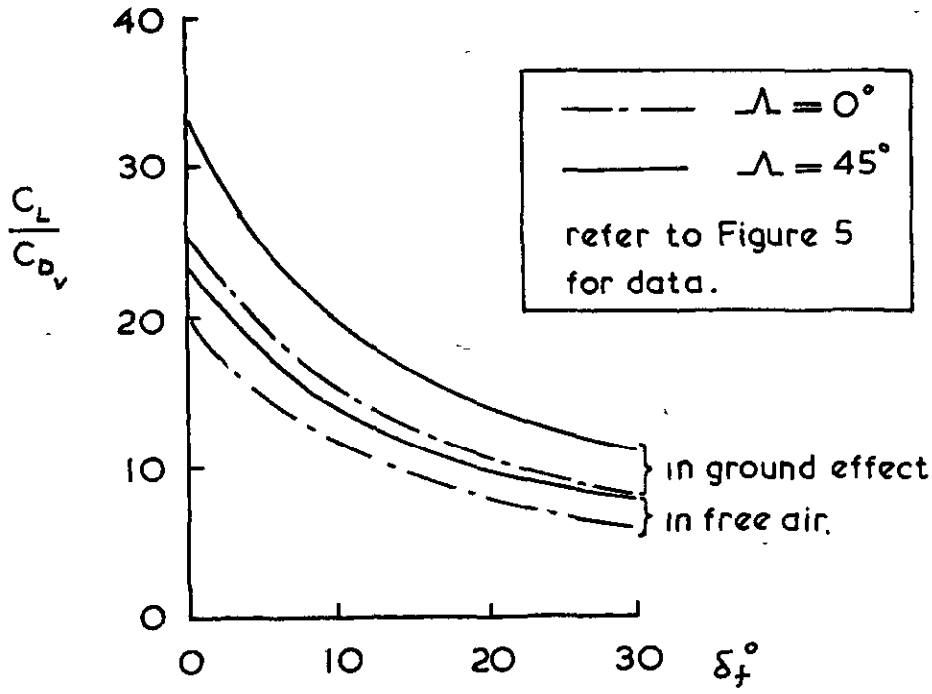

a) Variation of C_L/C_{DV} with flap deflection in free air and in ground effect.

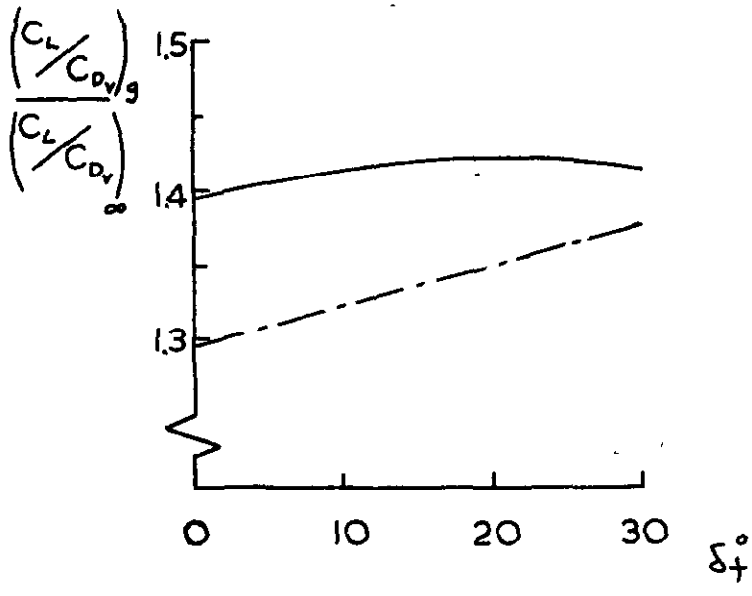

b) Relative ratio $(C_L/C_{DV})_g / (C_L/C_{DV})_\infty$ as a function of flap deflection.

Figure 12 CALCULATED RATIO C_L/C_{DV}

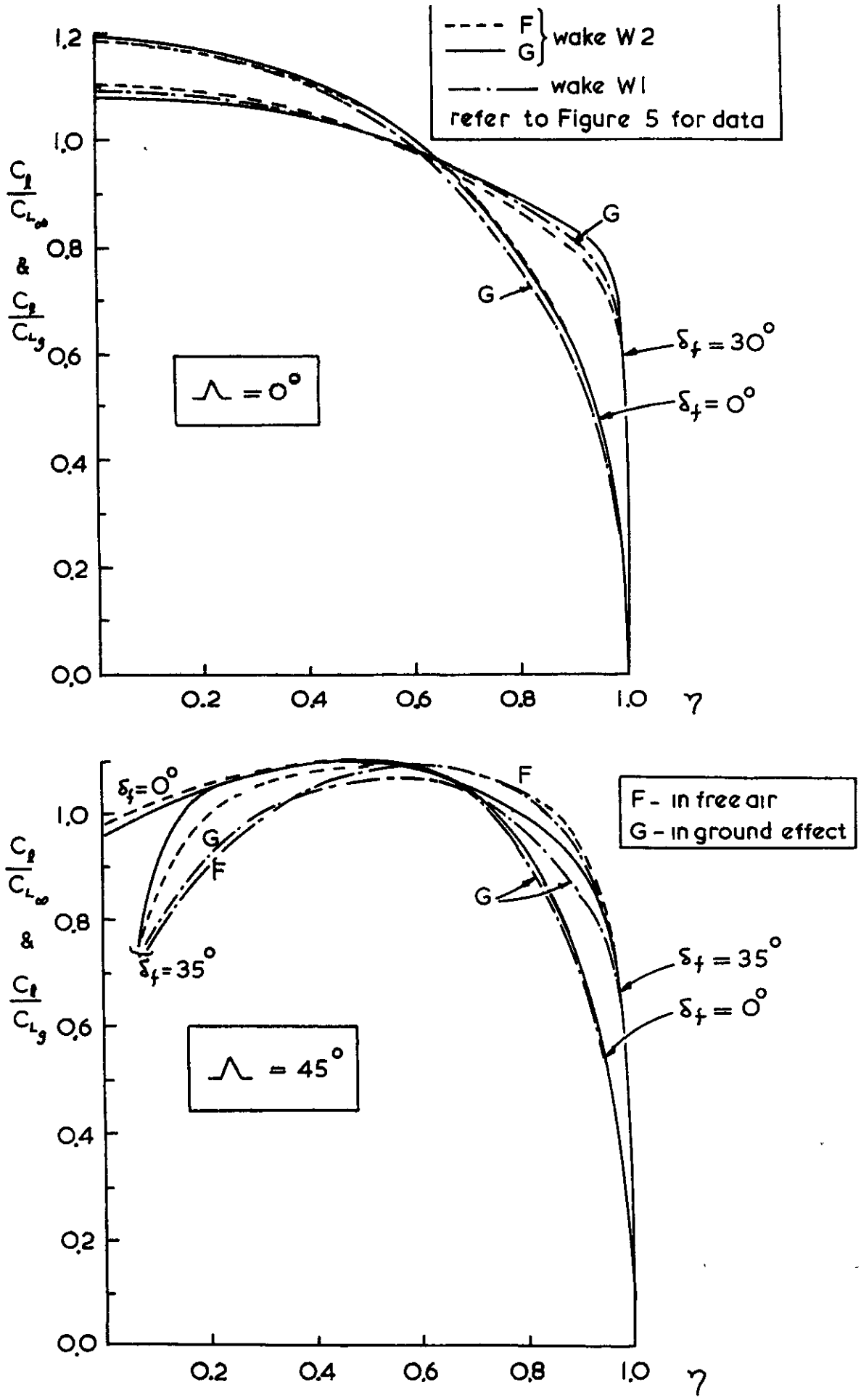

Figure 13 CALCULATED SPANWISE LOAD DISTRIBUTION FOR TWO SWEEP-BACK ANGLES.

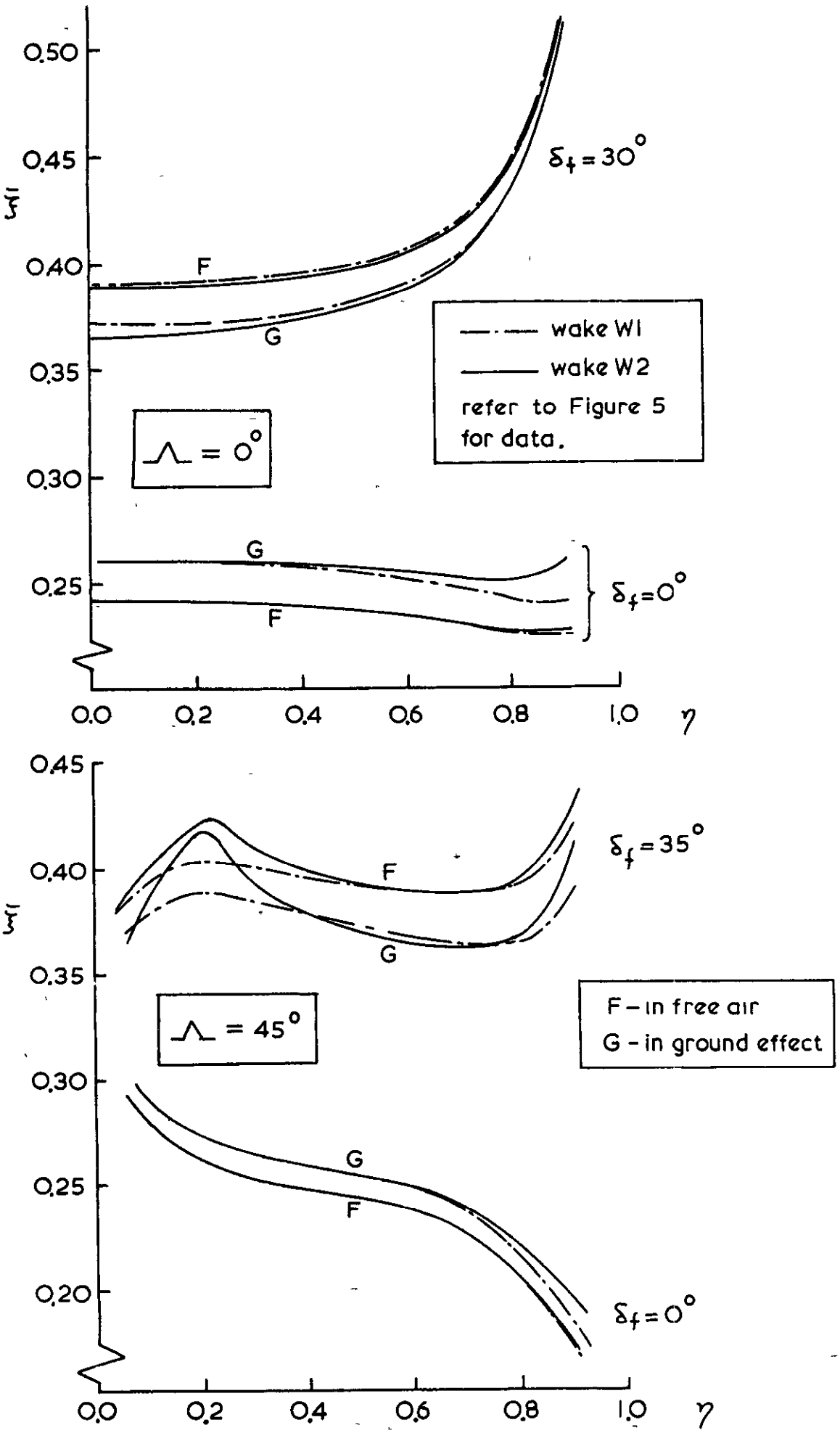

Figure 14 CALCULATED SPANWISE LOCUS OF CHORDWISE CENTRE OF PRESSURE FOR TWO SWEEPBACK ANGLES.

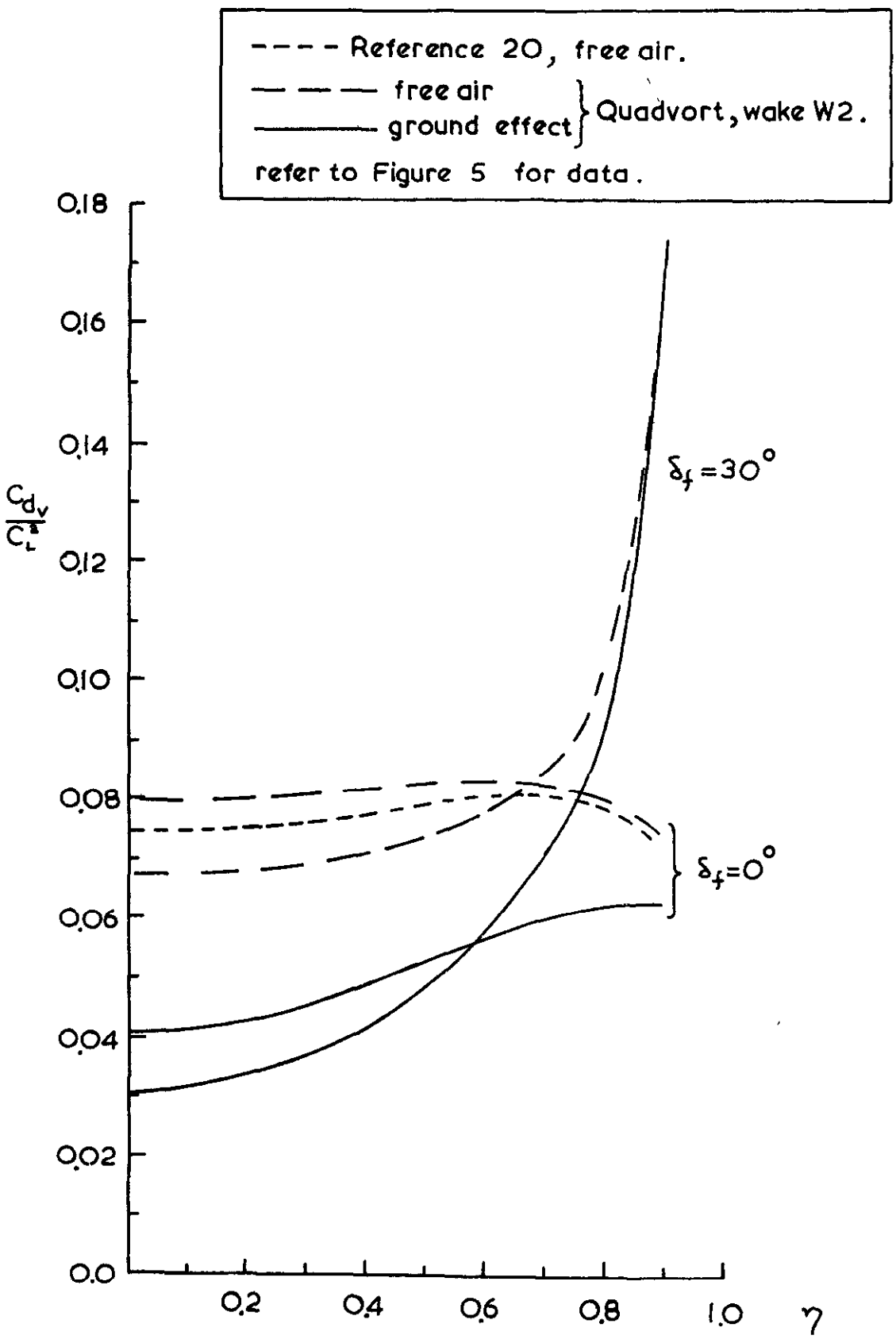

a) Zero sweepback

Figure 15 CALCULATED SPANWISE VARIATION OF VORTEX DRAG.

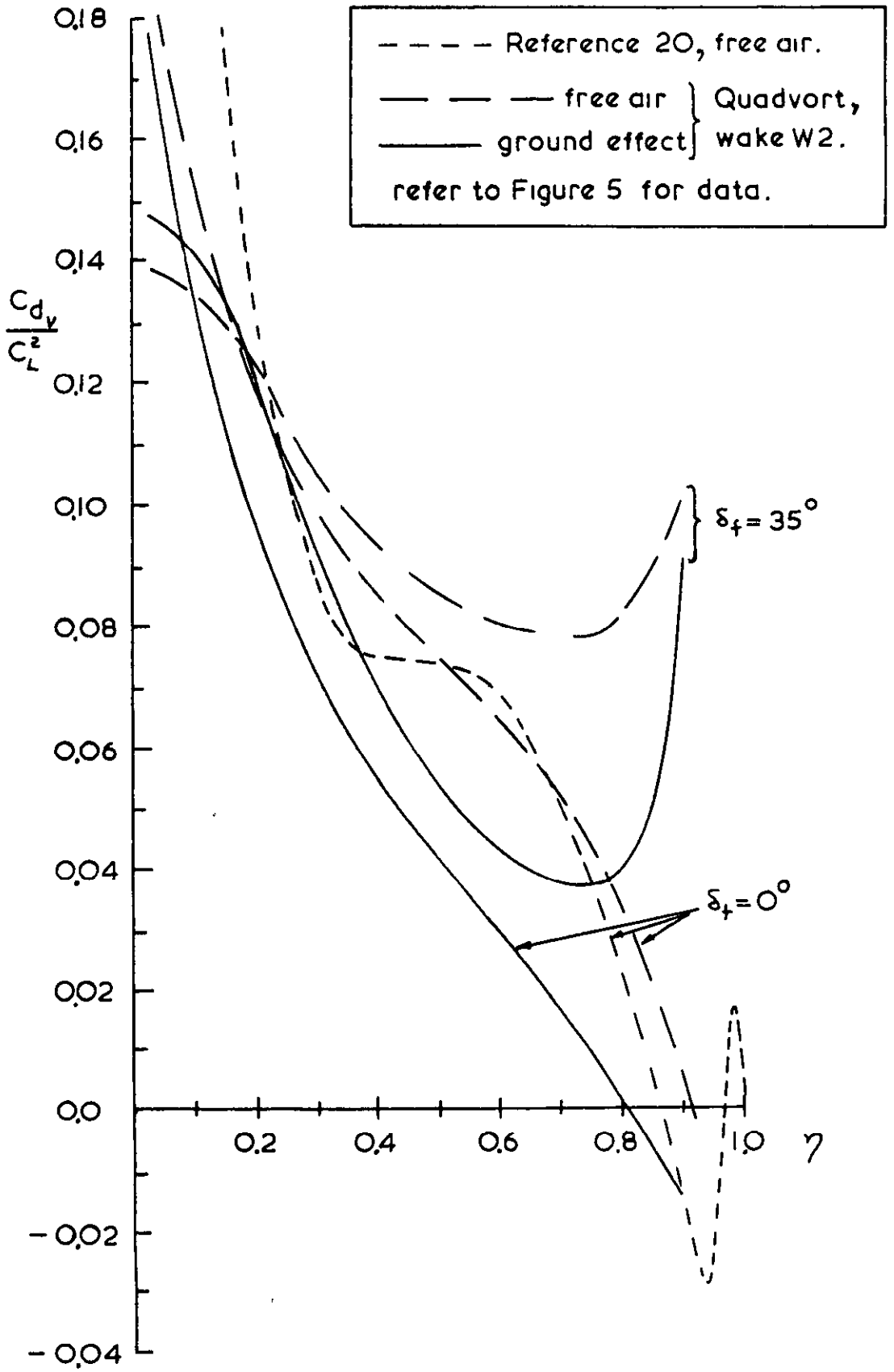

b) 45° Sweepback

Figure 15 CONCLUDED.

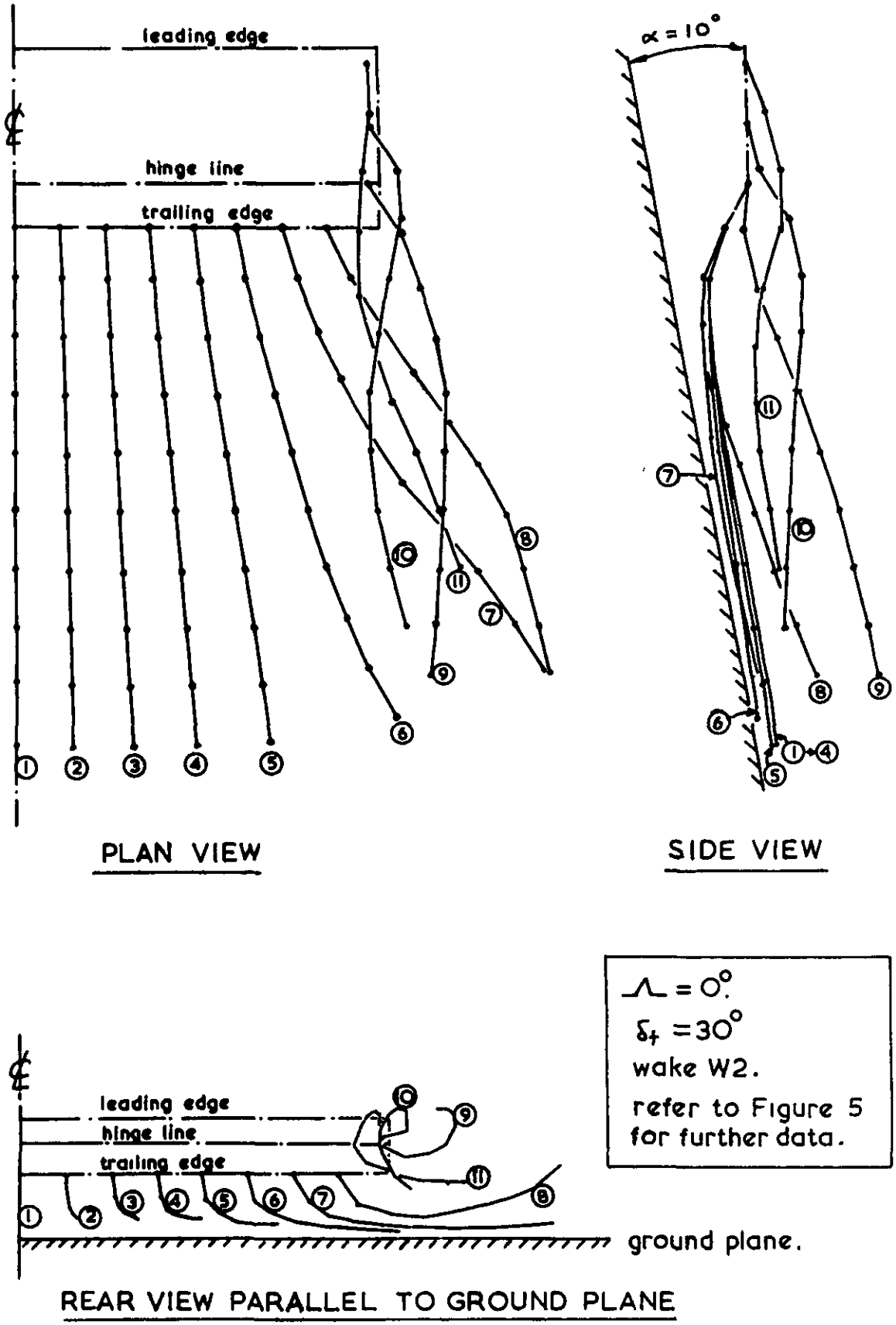

Figure 16 A TYPICAL CALCULATED VORTEX WAKE SHAPE.

HER MAJESTY'S STATIONERY OFFICE

Government Bookshops

49 High Holborn, London WC1V 6HB
13a Castle Street, Edinburgh EH2 3AR
41 The Hayes, Cardiff CF1 1SW
Brazennose Street, Manchester M60 8AS
Southey House, Wine Street, Bristol BS1 2BQ
258 Broad Street, Birmingham B1 2HE
80 Chichester Street, Belfast BT1 4JY

Government publications are also available through booksellers

C.P. No. 1264

ISBN 0 11 470822 3